remote sensing

MDPI

Review

Remote Sensing of Forest Burnt Area, Burn Severity, and Post-Fire Recovery: A Review

Eldar Kurbanov [1,*], Oleg Vorobev [1], Sergey Lezhnin [1], Jinming Sha [2], Jinliang Wang [3], Xiaomei Li [4], Janine Cole [5], Denis Dergunov [1] and Yibo Wang [1]

[1] Center for Sustainable Forest Management and Remote Sensing, Volga State University of Technology, Yoshkar-Ola 424000, Russia
[2] School of Geographical Science, Fujian Normal University, Fuzhou 350007, China
[3] Faculty of Geography, Yunnan Normal University, Chenggong District, Kunming 650500, China
[4] College of Environmental Science & Engineering, Fujian Normal University, Fuzhou 350007, China
[5] Council for Geoscience, 280 Pretoria Street, Silverton, Private Bag X112, Pretoria 0001, South Africa
* Correspondence: kurbanovea@volgatech.net

Abstract: Wildland fires dramatically affect forest ecosystems, altering the loss of their biodiversity and their sustainability. In addition, they have a strong impact on the global carbon balance and, ultimately, on climate change. This review attempts to provide a comprehensive meta-analysis of studies on remotely sensed methods and data used for estimation of forest burnt area, burn severity, post-fire effects, and forest recovery patterns at the global level by using the PRISMA framework. In the study, we discuss the results of the analysis based on 329 selected papers on the main aspects of the study area published in 48 journals within the past two decades (2000–2020). In the first part of this review, we analyse characteristics of the papers, including journals, spatial extent, geographic distribution, types of remote sensing sensors, ecological zoning, tree species, spectral indices, and accuracy metrics used in the studies. The second part of this review discusses the main tendencies, challenges, and increasing added value of different remote sensing techniques in forest burnt area, burn severity, and post-fire recovery assessments. Finally, it identifies potential opportunities for future research with the use of the new generation of remote sensing systems, classification and cloud performing techniques, and emerging processes platforms for regional and large-scale applications in the field of study.

Keywords: forest fire; remote sensing; burnt area; forest ecosystems; burn severity; post-fire forest recovery; meta-analysis

Citation: Kurbanov, E.; Vorobev, O.; Lezhnin, S.; Sha, J.; Wang, J.; Li, X.; Cole, J.; Dergunov, D.; Wang, Y. Remote Sensing of Forest Burnt Area, Burn Severity, and Post-Fire Recovery: A Review. *Remote Sens.* **2022**, *14*, 4714. https://doi.org/10.3390/rs14194714

Academic Editor: Dimitris Stavrakoudis

Received: 8 August 2022
Accepted: 14 September 2022
Published: 21 September 2022

1. Introduction

Wildland fires are periodic disturbance events that dramatically affect the structure and distribution of global forest ecosystems, altering soil erosion, causing loss of biodiversity, habitat, production and productivity, endangering human life, and disrupting livelihoods [1]. Over the past two decades, 7.20 billion ha of land was burned globally by wildland fires at an average of 400 million ha annually [2]. According to an analysis by the Food and Agricultural Organization, between 2001 and 2019, forest (tree-covered) areas accounted for about 29% of the total area burnt by wildfires [3]. The largest burnt tree-covered area in the total wildland fire area was in Central America (47%), while the smallest was in the Oceania region (2%) [3].

Furthermore, wildland fires have a strong influence on climate change due to the rapid release of carbon sequestered in forest biomass into the atmosphere [4,5]. In recent decades, the rapidly changing climate has increased the frequency and severity of wildland fires [6–10], and it is projected that further warming effects will likely cause more dramatic consequences to the forests, and an increase of burnt area (BA) [11–15]. Growing concerns about the impact of climate change has increased the need for the development of

sustainable forest management policies aiming to mitigate greenhouse gas emissions and increase the efficiency of fire management [16–18]. Broad scale severity levels at which fire affects a forest cover is a key factor for the successful assessment of post-fire impact and the strategy that promotes natural regeneration, as well as for understanding the effects of climate change on ecosystems [19,20]. Thus, comprehensive burnt area, burn severity (BS), and post-fire recovery monitoring and assessments are a critical tool for researchers, foresters, and fire managers.

Over the last few decades, the use of space-borne sensor data has provided unique advances for the professional community to detect forest ecosystem disturbances, especially for estimations of spatio-temporal fire dynamics and BA mapping [21,22]. Remote sensing (RS) techniques become an unprecedented alternative option to expensive and time-consuming field measures in the monitoring of forest ecosystems over large and remote geographic areas [23–26]. Multi-temporal satellite images of broad spatial resolution have been extensively used in measurements of forest areas prior to and post-fire acquisitions to map BA at regional and global scales [27–30], and to estimate burn severity [31–34] and vegetation recovery [35–38].

Given its importance for monitoring forest ecosystems and environmental management policies, the main objective of this paper is a review of state-of-the-art remotely sensed methods and data for estimation of forest BA, BS, and forest recovery patterns at the global level that have been applied in the research papers published in English in peer-reviewed scientific journals within the period between 2000 and 2020. The paper analyses current research trends and summarizes the application of remote sensing techniques for the burnt forest area, burned severity, and post-fire recovery. Finally, we recommend future research for the use of the new generation of RS systems, classification, and cloud performing techniques, and emerging process platforms for the regional and large-scale applications in BA studies.

2. Materials and Methods

2.1. Search Methodology

A systematic approach of a literature review from 2000 to 2021 was used in this research with a focus only on scientific peer-reviewed papers in the fields of BA, remote sensing, and forest ecosystems at the local, regional, and global levels. We selected this timeframe for two reasons. First, research in the field of applications for remote sensing and estimation of forest ecosystems and wildfires has prominently increased, especially in recent decades due to a rapidly growing number of Earth observation data sources. The progress of forest BA, BS, and post-fire recovery estimations from coarse resolution satellites to high spatial and temporal sensors was studied in the review. Second, during the last two decades, there were several comprehensive reviews from different parts of the world demonstrating a growing interest in the field of study among the professional community [39–44].

In order to perform the systematic review, we adopted the Preferred Reporting Items for Systematic Reviews and Meta-Analysis (PRISMA) framework [45]. The procedure of identifying, selecting, and analysing relevant articles based on PRISMA is given in Figure 1. The presented schematic diagram follows four phases: identification, screening, eligibility, and inclusion. The PRISMA 2020 checklist (https://www.mdpi.com/editorial_process#standards, accessed on 19 September 2022) comprises a report of several sections with a title, abstract, introduction, methods, results, discussion, and other information. Each PRISMA section consists of specific formulated questions to be identified and analysed in the selected research articles.

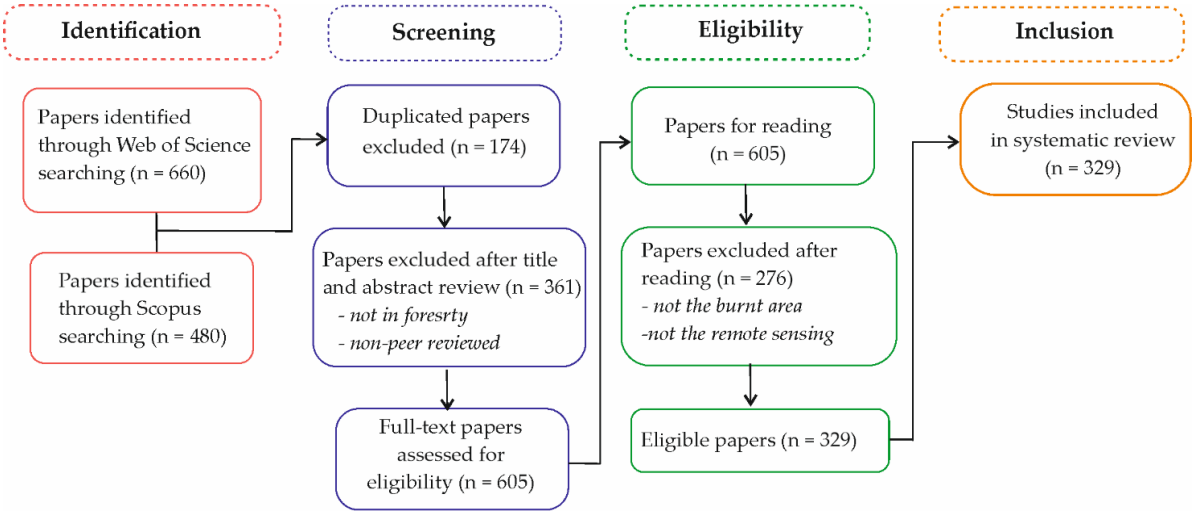

Figure 1. The schematic diagram of the papers selection order from 2000 to 2020 in the field of remote sensing of forest BA, BS, and post-fire recovery in the Preferred Reporting Items for Systematic Reviews and Meta-Analysis (PRISMA) framework.

Following that, a representative set of keywords were defined for the initial search in the electronic databases Scopus (Elsevier) and Web of Science (Clarivate Analytics): "remote sensing", "forests", "post-fire", "burnt area", "burn severity". A further search was carried out in the same databases using alterations in the keywords for specific satellites (MODIS, Landsat, Sentinel, etc.). The initial attempt showed that 1140 scientific publications were identified consistently with the designated search criteria, of which 660 papers were identified through the Web of Science, and 480 were found in the Scopus database (Figure 1). During the screening phase, the articles search was refined by removing the duplicates from the two databases. Further selection was made by reading the abstracts of the papers to identify research focusing on remote sensing techniques for monitoring and estimation of post-fire forest areas. If the abstract did not clearly describe that the study was related to forest BA, we continued to review the full text to identify the objective and methodology of the article. We also excluded non-peer reviewed publications, and articles where fires have affected other ecosystems (grasslands, shrublands, agricultural lands, meadows etc.). However, this was not always possible due to the fact that, in some regional and global studies, forests were classified along with many other land cover types.

At the eligibility phase, the full text of the remaining 605 articles were carefully reviewed based on the following criteria:

- Remote sensing techniques are the main components of the study;
- Study should attempt temporally explicit estimation of the forest BA and BS using different datasets for the validation of mapping results;
- Paper appropriately describes the methods and/or results of the study so that they can be interpretable and replicated;
- Focus is made on the forest stands rather than other ecosystem attributes (soils, water, undergrowth);
- Study should report detailed accuracy assessment results.

2.2. Data Compilation

Finally, 329 papers were shortlisted according to their suitability to the review and fitting of the search criteria, and organized in the reference management Mendeley platform (https://www.mendeley.com/, accessed on 10 May 2022) to conduct further meta-analysis. Details from the selected pool of publications were then extracted and compiled in several different categories related to geographic region (FAO Global Ecological Zone) of the study area, sensor used, spatial extent of the forest fire, temporal scale of the study, type of burnt forest (main

tree species), classification and modelling approaches, vegetation indexes, accuracy method used, year of the publication, and reference (validation) data. The complete list of described categories for each selected paper is provided in the Supplementary Materials (Table S1).

3. Descriptive Analysis

3.1. Publication Details

The number of studies conducted in the field of remote sensing of forest BA, BS, and post-fire recovery has increased substantially, as is evident from the number of articles published between 2000 and 2020 (Figure 2). This is well-supported by the general trend of increased publication activity in the field of remote sensing, availability, and open access policy for the Earth Observations data (https://www.earthobservations.org/open_eo_data.php, accessed on 10 May 2022), and the importance of the prevention of wildfires for sustainable forest management actions [1,3]. Within the decade 2000–2010, we selected 122 (38%) publications for further review, while during 2011–2020, the number was almost doubled, with 204 (62%) publications.

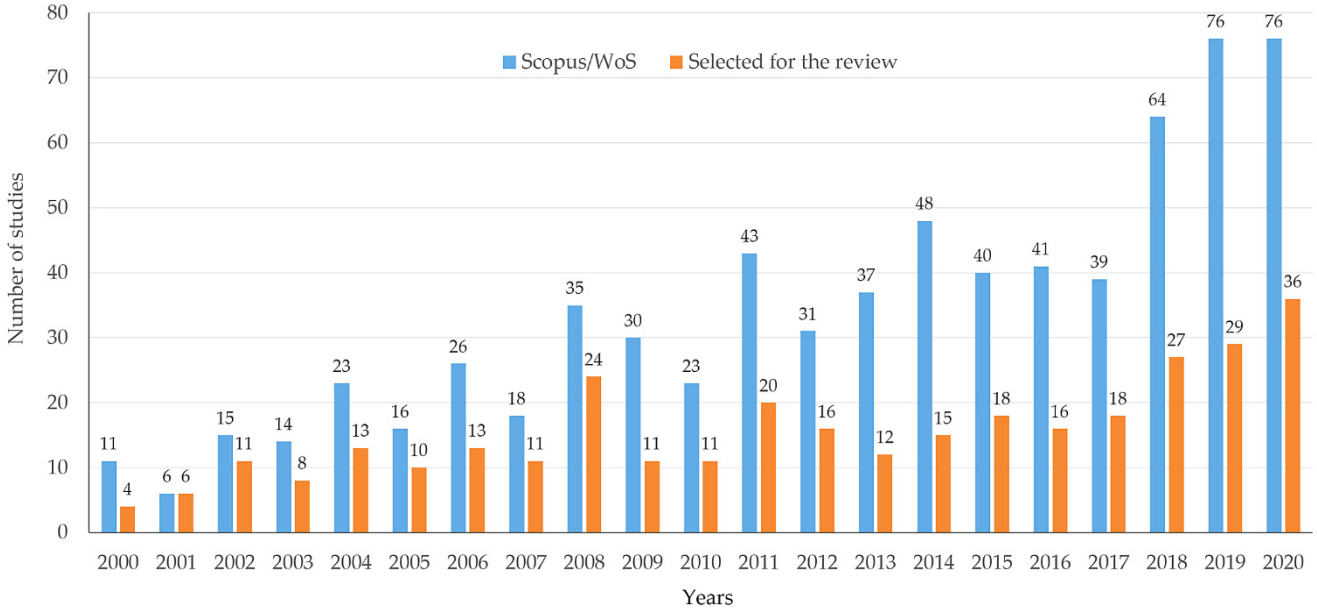

Figure 2. Temporal distribution of available and selected publications from 2000 to 2020 for the review in the field of remote sensing of forest BA, BS, and post-fire recovery, obtained from Scopus and Web of Science databases.

Data analysis revealed that 48 peer-reviewed journals published the selected papers. The main source journals of the 329 papers were: *Remote Sensing of Environment* (74 papers), *Remote Sensing* (56 papers), *International Journal of Remote Sensing* (39), *International Journal of Wildland Fire* (26), *International Journal of Applied Earth Observation and Geoinformation* (15), and *Forest Ecology and Management* (14) ranked as the top seven journals that published no less than 10 research articles during the past two decades.

The top 20 journals are presented in Figure 3, which together contained 285 publications or approximately 88% of the selected papers. The other 28 journals (12%) that published only two relevant articles were eliminated from the descriptive statistics in Figure 3. Most of them, which do not directly deal with remote sensing, were distributed across a wide range of journals (e.g., *Journal of Biogeography*, *Fire Ecology*, *Ecological Indicators*, *Climatic Change*, *Landscape and Urban Planning*, *Biogeosciences*, *Floresta*, *Ecological Modelling*, *Science of Total Environment*, *Global and Planetary Change*, *Contemporary Problems of Ecology*, *Izvestiya*, *Atmospheric and Oceanic Physics*, *Biological Conservation*, *Catena*, *Journal of Tropical Ecology*, *Environmental Monitoring and Assessment*, *Geophysical Research Letters*, etc.).

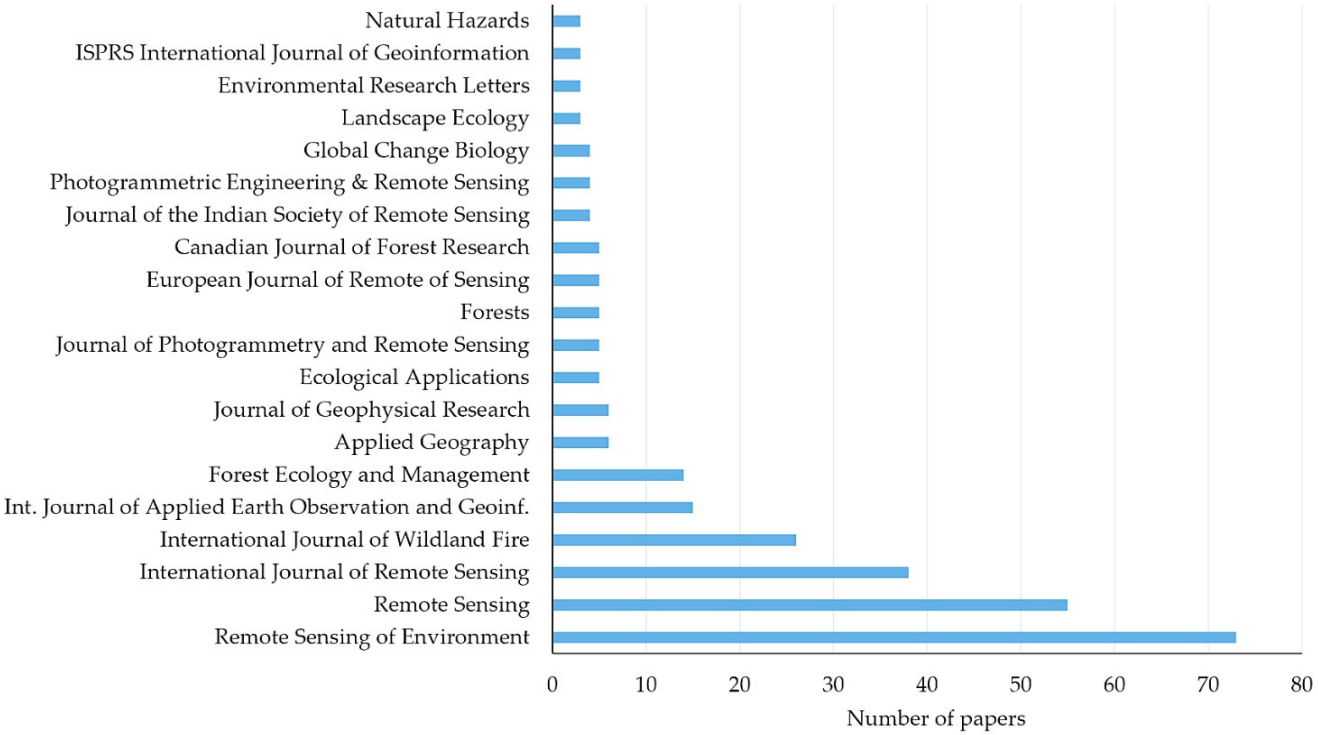

Figure 3. Top 20 out of 48 peer reviewed journals where the selected papers were published.

3.2. Spatial Extent and Geographical Distribution

The reviewed articles were categorized into five classes of spatial extent: local, multi-local, regional, national, and global scale. In this review, we define local scale as the level of forest unit (national park, forest district, forest reserve, etc.). Locations distributed across a country, different countries or continents without a specific spatial extent are referred to as the multi-local level. The regional level includes research at multiple locations within or across several provinces (states) of the country or cross-border studies in several countries. The national spatial level examines burnt forest within the state boundaries of the study country. Studies at the worldwide level were categorized as global scale. The statistical analysis indicated that the majority of the reviewed articles were conducted on the local (48%) and regional spatial scales (28%) (Figure 4). We identified 30 national (9%) and 28 multi-local (9%) scale studies of forest burnt area with the use of remote sensing, as well as 18 global studies (6%).

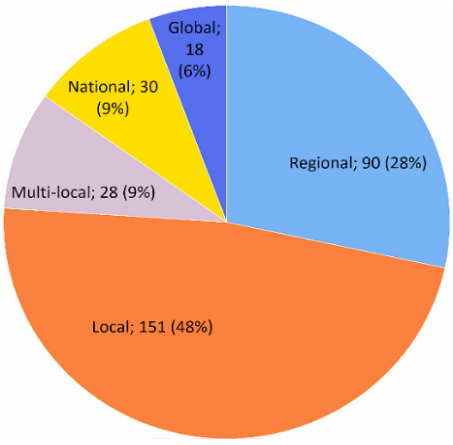

Figure 4. Distribution of selected articles at different spatial scales.

The studies considered in this review were conducted in many forest sites across the world including countries from America (North, Central, and South), Europe, Asia, Australia, and Africa (Figure 5a). Selected publications from 2000 to 2020 focused on forest fires in 39 countries. Journals with 10 or more publications originate from the USA (93), Spain (49), Canada (29), Greece (21), Brazil (17), Russian Federation (15), Italy (13), Portugal (12), Australia (10), and the People's Republic of China (10) (Figure 5b). In total, 269 articles (84%) described different approaches to the estimation of forest burnt area in ten of these countries with the use of remote sensing techniques. The case studies carried out in the USA, Spain, and Canada cover about 53% of all the reviewed publications. Other countries with more than two publications are also worth mentioning, particularly India (7), France (5), South Africa (4%), the Republic of Congo (3), Indonesia (2), South Korea (2), Turkey (2), Argentina (2), Malaysia (2), Peru (2), Israel (2), Chili (2), and the Central African Republic (2) (Figure 5b).

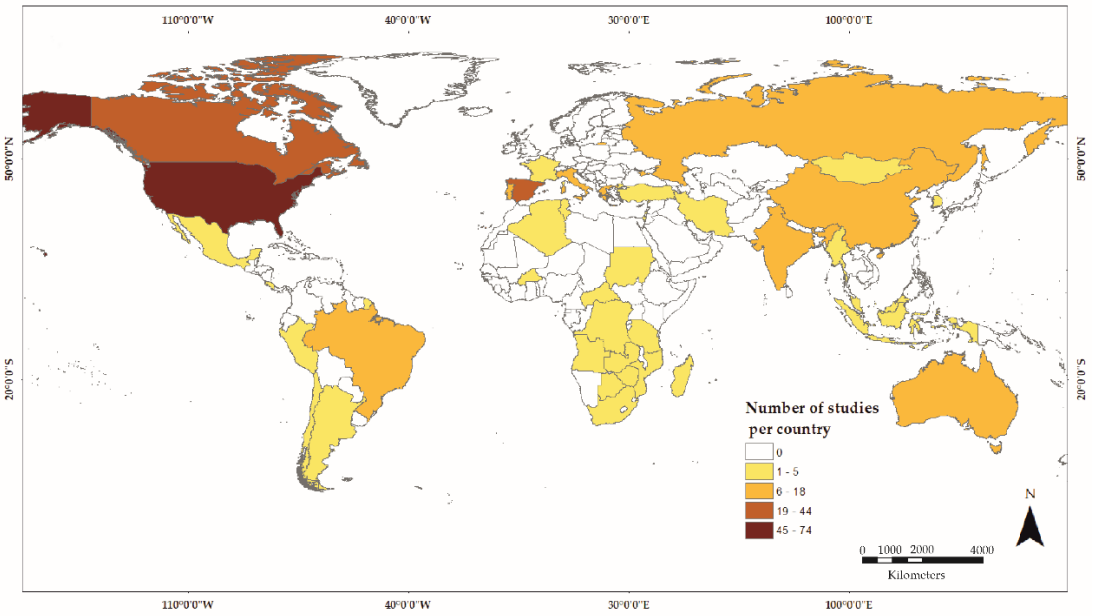

(**a**)

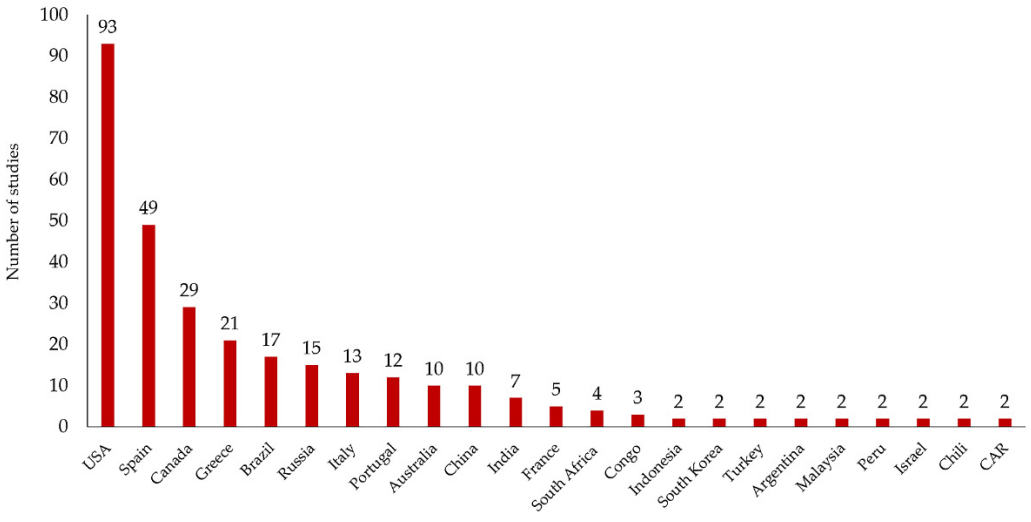

(**b**)

Figure 5. Geographic distribution of study site locations conducted per country: (**a**) global map of reviewed studies; (**b**) total number of studies per country (>1).

3.3. Sensor Type

In the study, we also analysed how often particular sensor types and satellite systems were used in the estimations. The reviewed studies were based on various applications of Earth observation data received from 30 different remote sensing sensor systems. The dominant applications were using optical sensors (264 cases, 80%), followed by thermal (Modis) (21%), LiDAR (7%), synthetic aperture radar (SAR) (5%), and aerial photo data (2%) (Figure 6a).

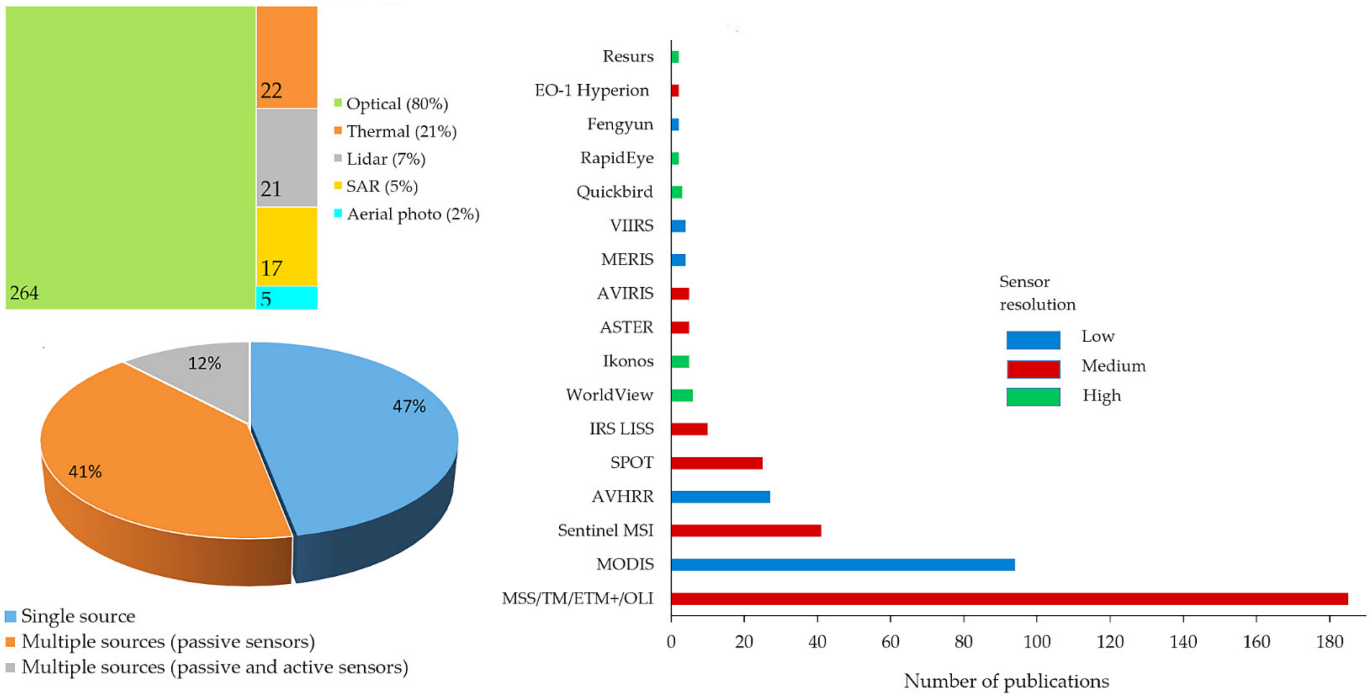

(**a**)-(**b**) (**c**)

Figure 6. Remote sensing sensor types and sensor systems used in selected publications: (**a**) number of sensor types applied; (**b**) sensors combination; (**c**) distribution of optical sensor system used in the studies.

Figure 6b shows the distribution of cases that use single or multiple remote sensing data sources. Almost half of the reviewed studies (154, 47%) used a single data source in their studies. In order to enhance the accuracy of forest burned area, another 41% of the studies used multiple optical data sources. About 12% of the studies used a combination of optical data and data from active sensors such as ALOS PALSAR and LiDAR.

In order to assess satellite sensors, we discussed three classes of spatial resolution: low (larger than 30 m), medium (5–30 m), and high (under 5 m). The most frequently used optical sensor type (185 cases, 40% of all studies) were multispectral Landsat systems of medium resolution, such as the Multispectral Scanner System (MSS), Thematic Mapper (TM), Enhanced Thematic Mapper Plus (ETM+), and the Operational Land Imager (OLI) (Figure 6c). The next image sources of medium resolution for burnt area studies mainly came from multispectral sensors including the Sentinel Multispectral Instrument (MSI) (41 cases or 8.9%), multiple sensors of SPOT satellite (25 cases, 5.2%), Linear Imaging Self-Scanning Sensors (LISS) of Indian ResourceSat family satellites (10 cases, 2.1%), the Advanced Spaceborne Thermal Emission and Reflection Radiometer (ASTER) of Terra satellite (5 cases, 1.1%), and the Airborne Visible InfraRed Imaging Spectrometer (AVIRIS) (5 cases, 1.1%). In terms of remote sensing imagery with low resolutions, the commonly used data sources were the Moderate Resolution Imaging Spectroradiometer (MODIS) (94 cases, 20.2%) on board of Terra and Aqua satellites, the Advanced Very-High-Resolution Radiometer (AVHRR) (27 cases, 5.2%), the Visible In-

frared Imaging Radiometer Suite (VIIRS) (4 cases, 0.9%), and the Envisat Medium Resolution Imaging Spectrometer (MERIS) (4 cases, 0.9%). Few studies were conducted with the use of high spatial resolution systems such as WorldView (6 cases, 1.3%), Ikonos (5 cases, 1.1%), Quickbird (4 cases, 0.9%), and Resurs (2 cases, 0.4%).

3.4. Referred FAO Ecozones and Tree Species

When considering the FAO Global Ecological Zone map (http://foris.fao.org/static/data/fra2010/ecozones2010.jpg, accessed on 20 May 2022) for defining forest regions of the world, most of the reviewed studies were conducted within subtropical dry forest (21.4%, 92 cases), followed by boreal coniferous forest (9.3%, 40 cases), boreal tundra woodland (8.4%, 36 cases), temporal continental forest (8.4%, 36 cases), and temperate oceanic forest (7.7%, 33 cases) (Figure 7a). Many studies were also focused on the subtropical mountain system (7.5%, 32 cases), the boreal mountain system (6.3%, 27 cases), the temperate mountain system (4.7%, 20 cases), the tropical rainforest (5.6%, 24 cases), and the temperate steppe (4.4%, 19 cases). Fewer studies were carried out in tropical mountain system (1.4%, 6 cases), subtropical desert (1.2%, 5 cases), tropical shrubland (0.9%, 4 cases), and temperate desert (0.7%, 3 cases). To some degree, the global distribution of the research forest sites within the FAO ecozones indicate spatial similarities between the locations of BA around the world.

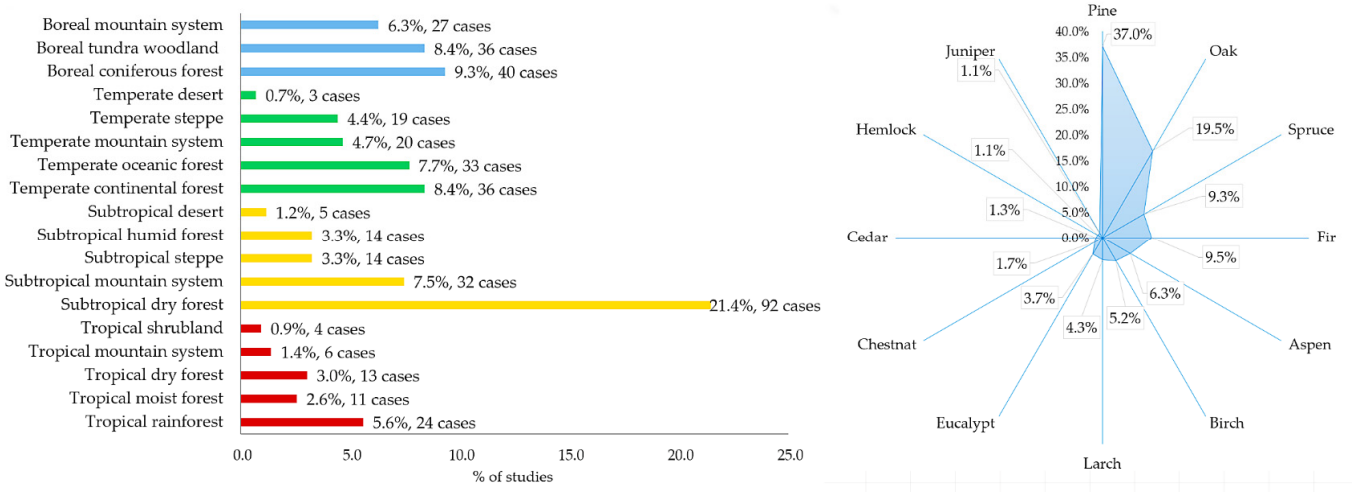

Figure 7. Distribution of studies: (**a**) according to the Global Ecological Zoning framework; (**b**) by the main tree species on the burnt sites.

With regard to forest tree species discrimination, the reviewed studies have mainly described pine (37.0%), followed by oak (19.5%), fir (9.5%), spruce (9.3%), aspen (6.3%), birch (5.2%), larch (4.3%), eucalypt (3.7%), chestnut (1.7%), cedar (1.3%), hemlock (1.1%), and juniper (1.1%) (Figure 7b). Among the 28 pine species described in the articles, the most often mentioned were Ponderosa pine (*Pinus Ponderosa*) (26 cases), Maritime pine (*Pinus pinaster*) (24 cases), Black pine (*Pinus nigra*) (19 cases), Scots pine (*Pinus sylvestris*) (15 cases), Aleppo pine (*Pinus halepensis*) (14 cases), Lodgepole pine (*Pinus contorta*) (11 cases), Turkish pine (*Pinus bruita*) (5 cases), and others (Table 1). Among the 32 oak species, the most frequently studied were Evergreen oak (*Quercus ilex*) (18 cases), Cork oak (*Quercus suber*) (10 cases), Kermes oak (*Quercus coccifera*) (8 cases), and others. Sixteen studies were exclusively examining BA covered by the black spruce (*Picea Mariana*), 19 studies estimated Douglas fir (*Pseudotsuga menziesii*), and 17 were focused on the trembling aspen (*Populus tremuloides*) forest stands. Furthermore, there were studies describing burnt territories dominated by Siberian larch (*Larix sibirica*) (9 cases), Dahurian Larch (*Larix gmelini*) (7 cases), and Siberian silver birch (*Betula Platyphylla*) (6 cases). Only four studies estimated blue gum (*Eucalyptus globulus*) and Darwin stringybark (*Eucalyptus tetrodonta*) species.

Table 1. Tree species on the burnt sites described in more than four cases (156 articles in total).

Tree Species	Number of Studies	Tree Species	Number of Studies
Ponderosa pine (*Pinus ponderosa*)	26	Siberian larch (*Larix sibirica*)	9
Maritime pine (*Pinus pinaster*)	24	Dahurian Larch (*Larix gmelini*)	7
Black pine (*Pinus nigra*)	19	Evergreen oak (*Quercus ilex*)	18
Scots pine (*Pinus sylvestris*)	15	Cork oak (*Quercus suber*)	10
Aleppo Pine (*Pinus halepensis*)	14	Kermes oak (*Quercus coccifera*)	8
Lodgepole pine (*Pinus contorta*)	11	Pyrenean oak (*Quercus pyrenaica*)	8
Turkish pine (*Pinus brutia*)	5	Downy oak (*Quercus pubescens*)	5
Jack pine (*Pinus banksiana*)	5	Portuguese oak (*Quercus faginea*)	4
Jeffrey pine (*Pinus jeffreyi*)	5	Douglas fir (*Pseudotsuga menziesii*)	19
Siberian pine (*Pinus sibirica*)	4	Subalpine fir (*Abies lasiocarpa*)	6
Pitch pine (*Pinus rigida*)	4	White fir (*Abies concolor*)	5
Stone pine (*Pinus pinea*)	4	Trembling aspen (*Populus tremuloides*)	17
Sugar pine (*Pinus Lambertiana*)	4	Common aspen (*Populus tremula*)	6
Longleaf pine (*Pinus palustris*)	4	Siberian silver birch (*Betula Platyphylla*)	6
Black spruce (*Picea Mariana*)	16	European white birch (*Betula pendula*)	5
White spruce (*Picea glauca*)	12	American white birch (*Betula papyrifera*)	5
Siberian spruce (*Picea obovata*)	4	Blue gum (*Eucalyptus globulus*)	4
Engelmann spruce (*Picea engelmannii*)	5	Darwin stringybark (*Eucalyptus tetrodonta*)	4

4. Results and Discussions

4.1. BA and BS Estimates

4.1.1. Spectral Indices and Mapping Techniques

The remote sensing of forest BA mapping has a long history, starting in the early 1970s, and during 2000–2020, it is still an active research topic employing advanced techniques that integrate geo-statistics, as well as object-oriented and machine learning methods [46]. During the last two decades, a wide range of products have been developed and applied in BA mapping at the global, regional, and local scales [47–64].

A reduction in the visible-to-near-infrared reflectance of vegetation cover and an increase in the short and middle infrared surface reflectance of most satellite sensors that occur following a wildfire can facilitate the identification of BA patterns [42,65–68]. Among the commonly used optical features, vegetation indices (VI) play a major role in the studies of remote sensing of forest BA and BS. During two decades, the most frequently used VI compared to other indices was the normalized difference vegetation index (NDVI) (128 studies, 23.4%), followed by the delta Normalized Burn Ratio (dNBR) (81 studies, 14.8%), Normalized Burn Ratio (NBR) (77 studies, 14.1%), and the relative differenced Normalized Burn Ratio (RdNBR) (32 studies, 5.8%) (Table 2). A total of 34 studies (6.2%) employed the composite burn index (CBI) to correlate remote sensing data with field characteristics of burn severity observed after wildfire [45].

A number of studies have observed the enhanced vegetation index (21 cases, 3.8%), the burn area index (BAI) (18 cases, 3.3%), the normalized difference water index (NDWI) (17 cases, 3.1%), the mid-infrared burnt index (MIRBI) (12 cases, 2.2%), and the global environmental monitoring index (GEMI) (12 cases, 2.2%). In order to minimise soil background reflectance, the soil-adjusted vegetation index (SAVI) (13 cases, 2.4%), modified SAVI (MSAVI) (12 cases, 2.2%) and the char soil index (CSI) (6 cases, 1.1%) were also applied.

Table 2. Spectral indices used for the review.

Sensor	Index	Description	Temporal Period	Number of Studies	% of Total Studies
MSS, TM, ETM+, OLI, AVHRR, MODIS, MISR, IRS WiFS, QuickBird, Ikonos OSA, Sentinel-2 MSI, SPOT VGT, RapidEye REIS, GeoEye GIS, WorldView-2,3	NDVI	Normalised Differenced Vegetation Index	2000–2020	128	23.4
TM, ETM+, OLI, MODIS, QuickBird, MSI, VGT, REIS, WorldView-2/3	dNBR	Delta Normalized Burn Ratio	2005–2020	81	14.8
TM, ETM+, OLI, MODIS, QuickBird, MSI, VGT, REIS, WorldView-2/3	NBR	Normalized Burn Ratio 1 (ND4/7)	2005–2020	77	14.1
TM, ETM+, MSI, AVHRR, MODIS	CBI	Composite Burn Index	2005–2020	34	6.2
TM, ETM+, OLI, MSI	RdNBR	Relative Differenced Normalized Burn Ratio	2007–2020	32	5.8
ETM+, SPOT VGT, MODIS, QuickBird	dNDVI	Delta Normalised Differenced Vegetation Index	2006–2020	22	4.0
TM, ETM+, MODIS, WorldView-2/3	EVI	Enhanced Vegetation Index	2010–2020	21	3.8
TM, ETM+, MODIS, WorldView-2/3, IRS AWiFS, QuickBird	BAI	Burn Area Index	2002–2020	18	3.3
TM, ETM+, MSI, MODIS	NDWI	Normalized Difference Water Index	2003–2020	17	3.1
TM, ETM+, WorldView-2/3, QuickBird	SAVI	Soil Adjusted Vegetation Index	2002–2020	13	2.4
TM, ETM+, MODIS	GEMI	Global Environmental Monitoring Index	2002–2020	12	2.2
TM, ETM+, MODIS	MIRBI	Mid-Infrared Burnt Index	2006–2020	12	2.2
TM, ETM+, WorldView-2/3, QuickBird	MSAVI	Modified Soil Adjusted Vegetation Index	2012–2020	12	2.2
TM, ETM+, OLI	NBR2	Normalized Burn Ratio 2 (ND4/5)	2005–2020	9	1.6
TM, ETM+, MODIS	LST	Land Surface Temperature	2014–2020	8	1.5
TM, MODIS, WorldView-2/3	GeoCBI	Geometrically structured Composite Burn Index	2010–2020	7	1.3
TM, ETM+, MODIS, WorldView-2/3, MSI	LAI	Leaf Area Index	2008–2020	6	1.1
TM, ETM+	CSI	Char Soil Index	2012–2020	6	1.1
MODIS	BAIM	MODIS Burned Area Index	2009–2020	5	0.9
MSI, OLI	RBR	Relative Burn Ratio	2018–2020	5	0.9
ETM, SPOT VGT	SWVI	Normalized short-wave-based vegetation index	2002–2020	4	0.7
TM, ETM+	NBRT	Normalised Burn Ratio Thermal	2018–2020	4	0.7
AVHRR, MODIS	BBFI	Burned Boreal Forest Index	2012–2020	3	0.5
TM, ETM+, WorldView-2	RVI	Ratio Vegetation Index	2012–2020	3	0.5
TM, ETM+, OLI	DI	Disturbance index	2014–2020	3	0.5
TM, ETM+	BSI	Burn Scar Index	2011–2020	3	0.5
TM, ETM+	NDII	Normalized Difference Infrared Index	2014–2020	3	0.5

In early 2000, the use of AVHRR, MODIS, IRS, SPOT/HRVIR, and Landsat to detect hotspots based on dNDVI images has been widely applied to estimate BA in many studies [69–83]. Confirmed hotspots are then used to derive regional-level NDVI difference thresholds for BA mapping. As an alternative to the NDVI, a non-linear global environmental monitoring index (GEMI) [84] provided better results for discriminating burned areas in several forest ecosystems [85–87]. The GEMI was specifically designed to minimize problems of contamination of the vegetation signal by extraneous factors to monitor recently burned areas. Another non-linear burnt area index (BAI), which integrates the minimum reflectance of burnt vegetation in the NIR and the maximum in the red bands,

was initially developed for BA discrimination in NOAA-AVHRR images [88]. The BAI was adapted to MODIS NIR and SWIR bands (BAIM) for mapping recently burned areas in Mediterranean ecosystems [89–91]. The mid-infrared bi-spectral index (MIRBI) [92], which applies to SWIR wavelengths, also showed strong spectral separation between burned and unburned areas [93,94]. Some researchers found that the MIRBI proved to be reliable to reduce confusions with mixed pixels found in water–land borders and areas affected by previous wildfires [28,95].

Several global BA detecting products have been developed over the past decades based on medium- and high-resolution sensors. Specifically, satellite data from the VEGETATION (VGT) sensor aboard the European SPOT-4 satellite were used to assess global BA based on large-scale vegetation features or seasonal burning activity in different ecosystems (boreal, tropical, wooded grassland, savanna, etc.) [96–98]. The GLOBSCAR project was initiated in 2001 as a part of the European Space Agency (ESA) Data User Programme, with the objective of producing global BA maps on the base of the Along Track Scanning Radiometer (ATSR-2) instrument onboard the ESA ERS-2 satellite [99]. The Globcarbon BA product (ESA project), which was developed at a spatial resolution of 1 km, 10 km, 0.250 m, and 0.50 m with monthly temporal resolution to focus on ten complete years (1998–2007), can be flexibly applied to existing archives and readily merged into Earth system models [100].

Two NASA BA products, MODIS MCD45A1 [101] and MCD64A1 [102], which map the spatial extent and approximate date of biomass burning worldwide at a spatial resolution of 500 m, have been validated with the use of Landsat scenes in southern Africa, western United States, and central Siberia. Both products were used to conduct a broad range of studies concerning forest fire estimates and biomass burning emissions [103–112]. The fire information for a resource management system (FIRMS) is also a useful product developed by NASA, delivering MODIS active fire data to forestry managers in more than 90 countries [113,114]. A new FireCCI50 BA product was developed within the European Space Agency's (ESA) Climate Change Initiative (CCI) programme [115]. The product was generated from the MODIS (2001-2016 archive) red (R) and near-infrared (NIR) reflectance and thermal anomaly data, providing the highest spatial resolution (250 m) among the existing global BA datasets.

In recent years, approaches to planetary-scale geospatial analysis of BA have emerged by using a cloud-based Google Earth Engine (GEE) platform with several satellite data catalogues at different spatial resolutions (MODIS, Landsat, and Sentinel-2). In order to provide higher accuracy and detect small, burned patches, a novel 30 m spatial resolution Global Annual Burned Area Mapping (GABAM 2015) technique was proposed based on a huge catalogue of Landsat time series imagery, as well as the high-performance computing capacity of GEE [116,117]. Cross-comparison with the Fire_CCI50 BA product showed a similar spatial distribution and a strong coefficient of determination (R^2 = 0.74) between the burned areas of the two products, particularly in coniferous forests [117]. Another version of a global automatic BA algorithm at medium spatial resolution of Landsat or Sentinel-2 reflectance images was also developed in GEE [118]. The proposed automatic algorithm has shown globally spatially and temporally coherent results and higher accuracy in the detection of smaller BA.

The growing number of global satellite-based BA products available for the international remote sensing community has led to the development of methods and validation protocols to estimate their accuracy metrics. Although over the last two decades there has been extensive research on the topic [47,119–121], the basis of global BA accuracy assessment has been built according to the "good practice" guidelines for land cover validation procedure [122]. The validation protocols for these products have not been formally produced. Therefore, the procedure and methodology rely on previous research publications and validation exercises [110,123,124]. Several studies compared the accuracy of the above global BA products, proving that there are substantial differences between them in many regions of the world [47,125–131]. Six global burned area products were compared using the same protocols and reference data [132]. While the overall accuracy (OA) in this study

exceeded 99% for all the products, the BA commission error ratio was above 40% for all products and the omission error ratio was above 65% for all products. A Bayesian algorithm (BY-MODIS) to detect BA, originally developed for the North American boreal forests, was compared with MODIS database BA products MCD64A1 Version 6 and MCD45A1 Version 5.1 for the 2002–2012 period in forest ecoregions of Spain [87]. The total BA distinguished by the BY-MODIS classifier was 78.6% according to the data obtained from the Landsat images, with the lowest average commission error (11%) out of the three products and a correlation (R^2) of 0.82 [87]. Meanwhile, the commission and omission errors of the GABAM-2015 machine learning classification were 13.17% and 30.13%, respectively, and the overall accuracy reached 93.92% according to preliminary global validation [116]. The GABAM product also detected the largest forest BA in Amazonia, followed by TREES (a regional BA product, developed particularly for the Amazon region), MCD64A1, and Fire_cci [133]. The above studies show that there is a need for global and regional products with higher spatial resolution to provide the most accurate BA estimation.

Among the analysed publications, there has been considerable interest regarding satellite-based assessments of BS pattern heterogeneity within the border of a forest fire. For the purposes of the present study, we defined BS as the degree to which an ecosystem has changed due to both short- and long-term wildfire effects [134,135]. Relative magnitudes of BS are often expressed in terms of specific forest ecosystem characteristics (vegetation, litter, and soil) that are visually ranked after fire occurrence [136,137]. In the context of remote sensing, BS usually refers to measurements made directly after the wildfire, including metrics such as canopy consumption and tree mortality [134] or consumption and charring of organic soil profiles [137,138].

The assessment of burn severity in the field is often based on direct measures of the composite burn index (CBI), which was designed to estimate severity in situ by rating the average burn condition on a field plot [134,139]. During the last two decades, CBI has been frequently used in many studies (Table 2) for validating different remotely sensed products and for comprehensive assessment of BS in a wide range of various forest ecosystems [32,140–154]. A drawback of the CBI is that it requires knowledge of the pre-fire conditions of the assessed area [136,141], and it does not account for differences in the fractional cover of each ecosystem stratum [155]. De Santis and Chuvieco [156] proposed a modified geometrically structured composite burn index (GeoCBI) to improve the retrieval of burn severity from remotely sensed data. It is an operational tool to visually assess the burn severity by fire on the ground in five forest strata (soils, understory vegetation, mid-canopy, overstory, and dominant trees). Several studies [157–160] reported that GeoCBI is more strongly correlated with spectral reflectance of vegetation on burned areas. Other studies have suggested that burned area and burn severity patterns can also be quantified using remotely sensed change in LAI and empirical models [161–166].

While NDVI is still used in current research, during 2005–2020 (see Table 2), the Landsat normalized burn ratio (NBR) has emerged to be meant for BS assessment of forestry wildfires using remote sensing technology [155–160]. The NBR (and difference NBR) incorporates information about the spectral changes at the surface using the differing responses of near-infrared (NIR, 0.76–0.90 mm) and mid-infrared (SWIR, 2.08–2.35 mm) bands to generate a scaled index of BS [134,167–171]. Calculated by subtracting the post-fire NBR from the pre-fire NBR, the dNBR approach produces a more accurate assessment of burn severity than the single NBR because it is based on the measurement of per pixel changes in reflectance, making the overall approach more transferable across ecosystems [172–180]. Delineating the calculated dNBR Landsat images and thresholding them into severity classes has formed the basis for the Monitoring Trends in Burn Severity (MTBS) program, whereby all wildfires larger than 200 ha are mapped at the national level [181–183]. Both the dNBR and dNDVI indices were accurate in detecting high severity in north Patagonian forests, but to a lesser degree for detecting moderate and low severity burns [184]. Epting et al. [185] evaluated 13 remotely sensed indices (single bands, band ratios, vegetation indices, multivariate components, normalized differences) for mapping burn severity in

interior Alaska, and concluded that post-fire NBR gave the best correlations with the field-based CBI in closed needleleaf, mixed, and broadleaf forest classes, followed by the dNBR. However, they warned that the relationship between the NBR and CBI was poorer in areas with sparse tree cover (open woods, scrub, herbs, and pastures).

dNBR provides a measure of absolute change, whereas RdNBR was developed as a relative measure to account for spatial variation in the pre-fire leaf area index and to improve estimations in areas with heterogeneous and non-productive vegetation cover [186–188]. There is no common consent among researchers regarding the use of each BS index in terms of forest ecosystems, terrain, and estimated scales. Some studies have concluded that RdNBR provides a more consistent measure of burn severity with higher classification accuracies than dNBR [189,190]. Other researchers have reported that the relationships between the NBR and its derivatives (dNBR and RdNBR) to burn severity are highly variable and inconsistent across the burned areas and ecosystem types (savanna, boreal and tropical forests) [191–194]. The study in southeast China showed that the dNBR is a more reliable index for wildfire burn severity mapping than the RdNBR, which resulted in higher R^2 and smaller RMSE values for the forest area [195]. Based on field data from six fires, a study in the Canadian National Parks revealed that dNBR had higher overall classification accuracy than RdNBR, and that fires with the lowest forest canopy closure and heterogeneity ranking showed no improvement with RdNBR [167]. The results of this research show that the RdNBR-derived model did not estimate burn severity more accurately than dNBR (65.2% versus 70.2% classification accuracy). In addition, the use of NBR or dNBR to assess burn severity may be difficult because of variations in topography and solar elevation angle over the course of the growing season [31,194]. The relativized burn ratio (RBR), which provides an alternative to dNBR and RdNBR, was proposed as a Landsat-based metric and evaluated for the wildfires in the conterminous western USA [196]. Their results show that the RBR outperformed the dNBR and RdNBR in overall accuracy and in correspondence with field-measured CBI. However, it has also been found out that in heterogeneous areas, with a high presence of shrubs and grass, there were minor differences among dNBR, RdNBR or RBR in estimating BS [197–199]. While all these standard spectral indices remain the most appropriate for estimating burn severity, there is no strong agreement among researchers regarding the strengths and weaknesses of each NBR-derived index [200–202].

Several studies have proposed the use of changes in land surface temperature (LST) and land surface albedo (LSA), as land surface biophysical parameters describing the balance of water and energy, for estimating the BA and BS of forest ecosystems [144,203–209]. All of the studies reported the expected temperature increase in the immediate post-fire environment. For example, NBR and three indices in which the NBR is enhanced with LST revealed the best performance in assessing burn severity in chaparral shrublands [210]. Maffei et al. [211], based on the time series of daily Aqua-MODIS LST data (2003–2017) and the harmonic analysis of time series (HANTS) algorithm, demonstrated that the LST anomaly is a covariate of both burned area and fire duration. The comparison of the above publications in relation to the burn severity may aid in better understanding of forest burn patterns at different spatio-temporal scales, as well as providing reliable information for forest managers' systematic monitoring of wildfires and restoration efforts.

4.1.2. Active RS Sensors

During the last decades, several techniques have been developed for using synthetic aperture radar (SAR) and LiDAR data for BA mapping and fire damage assessment in forested areas [125,149,163,212,213]. Unlike optical sensors, the radar data can be obtained around the clock, at any position of the sun and adverse weather conditions, including rain, smoke, and clouds, which is crucial in emergency situations. SAR uses microwave energy for BA mapping, given that the backscatter signal is sensitive to vegetation structure and forest biomass [214,215]. Radar-based measurements, such as polarimetric decomposition coefficients, interferometric coherence, and backscatter intensities, show satisfactory BA

estimation accuracies in wildfire-affected forests [134]. The detection of BA from SAR is based on ecological changes that occur after wildfire, including the removal of tree canopies, exposure of rough ground, and increased water content in the burned surface [216,217]. These changes are directly proportional to the degree of BA, appearing on SAR images as relatively darker objects compared with non-affected forest areas, particularly when rainfall occurs after the fire [218].

With the launch of ESA's Sentinel (S) satellite, SAR images are now easily accessible with systematic acquisitions at a 5 × 20 m spatial resolution, which largely increases the capacity of BA detection [219,220]. The combined use of the S1 SAR and S2 Multi Spectral Instrument (MSI) sensors made it possible to detect 36,000 ha of BA in Marantaceae forests of the Congo Basin, characterized by open tree canopy and a tall herbaceous layer [27]. A new approach in the use of Sentinel-1A and RADARSAT-2 data from different orbits demonstrated their good agreement and potential of a thresholded, multi-temporal, α-angle-based index (NDαI) for mapping BA in a fire-prone region of the Western Cape (SA) [221]. The study also revealed that large omission errors, correlating strongly with areas of high local incidence angle, could be minimised by the combined use of both datasets. Another study of BA detection and mapping in tropical and sub-tropical Africa based on two Sentinel-1 and one Sentinel-2 algorithms suggested that optical-based algorithms provide a significant increase in accuracy compared to radar-based algorithms [131].

Light detection and ranging (LiDAR) has recently emerged as a powerful tool for producing 3D forest structural attributes, mapping BA, and assessing post-fire regeneration [222–225]. Some studies have combined multispectral/hyperspectral data and LiDAR data to estimate BS patterns using analysis of tree height and forest canopy structure [226–231]. There has been only a few studies estimating the spatial-temporal match of pre- and post-fire LiDAR acquisitions to quantify BS on forest structure. Bishop et al. [232] assessed the accuracy of classifying colour-infrared imagery in combination with post-fire LiDAR, and with differenced (pre- and post-fire) LiDAR, in a second-growth coast redwood forest, CA. The research demonstrated a moderate increase in overall accuracy compared to the use of imagery alone; the model using NDVI and post-fire LiDAR was 85% accurate. Montealegre et al. [233] developed a methodological approach combining post-fire airborne LiDAR data and field assessed CBI to estimate BA in Spanish forests. Developed regression models confirm that classified maps of BA are acceptable up to 85.5% overall accuracy. Liu et al. [234] investigated the application of photon counting LiDAR data from NASA Ice, Cloud, and Land Elevation Satellite-2 (ICESat-2) to classify BA over forests in northern California and western New Mexico. The classification results indicate 83% overall accuracy of BA maps based on spaceborne LiDAR, Sentinel-2, and Landsat 8 derived samples [234].

While using airborne LiDAR data provides good potential for assessing BA and BS in forestry with high accuracy, nowadays, the application of these data over large areas is limited by its cost associated with data acquisition. Another drawback to the incorporation of LiDAR measurements for the purpose of BA estimations is the lack of up-to-date pre-fire data for most forestry areas. Nevertheless, the use of LiDAR in wildfire assessments is expected to increase based on the capability to provide high spatial resolution data.

4.2. Monitoring of Post-Fire Forest Recovery

Quantifying post-fire effects become increasingly significant for understanding how forest ecosystems respond, including vegetation recovery, patterns of succession, ecosystem resilience, ecological impact, and planning forest management [40,235,236]. In this respect, RS has been recognized as an indispensable tool for monitoring reforestation patterns after wildfire [237–241]. Among different quantitative techniques, Tasseled Cap [242] and Multitemporal Kauth Thomas transformations [243] are of particular interest to the researchers as they are based on assessing satellite imagery of three key indicators of post-fire vegetation conditions—brightness, greenness, and wetness. Numerous studies have used a comprehensive analysis related to both transformations for mapping changes and disturbances in forests after wildfires [244–250].

Several studies on post-fire dynamics have been carried out in boreal forest ecosystems using optical sensors. Hicke et al. [251] estimated a mean NPP post-fire recovery for North American boreal forests of about 9 years using a 17-year time series of AVHRR NDVI observations. Another study used two NDVI AVHRR 17-year time series datasets to investigate vegetation recovery after wildfire in the boreal forest of Canada [252]. The results indicated that the rate of forest recovery varied in three episodic wildfire years (1981, 1989, and 1995), and that recovery times to preborn levels (5 years or more) were shorter than in previous studies. Cuevas-Gonzales et al. [253] observed spatio-temporal patterns of the fraction of absorbed photosynthetically active radiation (fAPAR) with the use of the MODIS time series to estimate post-fire dynamics during and two years after a fire event in Siberian boreal forests. Their results indicated that the differences in the fAPAR trajectories are correlated with the forest type, and fAPAR changes are not significantly different among the boreal latitudinal regions. The post-fire regeneration of Siberian boreal forests was studied using a 16-year time series of NDVI and NDSWIR (normalized difference shortwave infrared index) derived from MODIS [35]. The results have proved that more than 13 years are needed for the temporal NDVI and NDSWIR signals to recover fully after wildfire. Epting and Verbyla [254] used Landsat TM/ETM+ images to estimate forest succession over a 16-year post-fire period in interior Alaska. The study results indicated that patterns of post-fire Alaskan boreal forests are strongly linked to both the types of pre-fire vegetation and BS. In sixteen years after the fire, most of the high BS areas with closed needle-leaf, open needle-leaf, and mixed forest classes shifted to woodland or shrubland [254]. Frazier et al. [255] used three spectral recovery metrics derived from an annual Landsat based per-pixel NBR time series to estimate the recovery cycles of Canadian boreal forests. They found that post-fire spectral forest recovery rates have increased during 1986–2011 by 18% in the Taiga Shield East and 9% in the Taiga Shield West of Canada.

Many studies of post-fire vegetation responses are based on the discrimination of spectral bands and vegetation indices (mostly NDVI, dNBR, and EVI) by MODIS, Landsat, SPOT, and Sentinel multitemporal imagery in different regions and forest ecosystems of the world [256–267]. Numerous studies have observed that NDVI has a higher correlation with post-fire vegetation regrowth, leaf area, and biomass than other VI [36,135,268]. Severe changes in the ecosystem growth conditions caused by forest fire often result in rapid reforestation processes that can be observed at the regional level with MODIS 250-m NDVI time series data [35,36,269–272]. Ryu et al. [273] used MODIS and Landsat TM/OLI data to evaluate forest recovery processes and physiological activity after the April 2000 forest fire on the eastern coast of South Korea. The study results show that the pine (*Pinus densiflora*) ecosystem conditions improved to the initial state 8 years after the fire event, while vegetation biomass required more time to recover. Meng et al. [274] also used changes in NDVI following thirty-five fires in mixed conifer forest in the Sierra Nevada Mountains of California between 1999 and 2006. They reported that post-fire drought has a significant effect on the recovery of burned mixed-conifer forest, while burned red fir forest was sensitive to post-fire temperature. Lee and Chow [275] found that vegetation rapidly recovered in the first three years (NDVI increased substantially) following the wildfire in Bastrop State Park (USA), but that recovery was still significantly delayed compared to the control plot of the field data. On the other hand, the NDVI curves performed differently when estimated by BS level, showing a net decline in heavy and moderate BS areas [275].

Post-fire recovery dynamics were assessed in Mediterranean pine (*Pinus halepensis* and *Pinus pinaster*) forests (Spain) using temporal segmentation of the Landsat time series (1994–2018) and trajectory metrics from Tasseled Cap Wetness (TCW) and Tasseled Cap Angle (TCA) [276]. The research suggests that pine forest recovery rates were highly correlated to post-fire climate in the mid- and long-term, and with BS in the short-term [276]. Several studies in modelling of forest recovery and regeneration rates adopted other significant factors such as vegetation type, underlying topography, soils, slope-aspect, rainfall, and drought indicators [277–279]. Zhao et al. [280] estimated post-fire forest

spectral recovery in the Greater Yellowstone Ecosystem (GYE) using the Landsat Time Series Stack-Vegetation Change Tracker (LTSS-VCT) algorithm and high spatial resolution images from Google Earth. They found that forest regeneration is highly correlated with forest type, elevation, and soil type of the GYE. Another study in Mediterranean forest ecosystems [281] demonstrated evidence that the number of ongoing wildfires within a short period decreased the forest recovery negatively measured as EVI, which was also influenced by micro-climatic effects (soil and environmental humidity). Such studies also suggest that results are more meaningful when other important factors are considered, modelled, and compared with the forest recovery on BA.

In addition to optical sensors, the value of using unmanned aerial vehicles (UAV), SAR, and LiDAR imagery for estimation and monitoring of post-fire forest recovery has also been demonstrated [282–285]. Padua et al. [286] reported that the efficiency of Sentinel-2 satellite data for post-fire forest regeneration monitoring in the north-eastern region of Portugal is more cost-effective than UAV data. Several studies confirmed that the combination of SAR and Landsat bands was essential for estimation of regeneration stages in different forest ecosystems [282,287,288]. Polychronaki et al. [259] estimated post-fire vegetation recovery on the Mediterranean island of Thasos using multi-temporal SPOT and European Remote-Sensing (ERS) (C-band VV) images covering the period from 1993 to 2007. Results showed that the use of the ERS backscatter coefficient reduced the commission errors almost by half when mapping the forested areas recovery in Thasos [259].

LiDAR stands out as an important technology capable of being directly associated with ecosystem biomass and post-fire changes on the local level, since it measures the three-dimensional structures of forest cover. Sato et al. [289] estimated post-fire changes in forest canopy height and biomass using airborne LiDAR in western Amazonia. Their results indicated that even ten years after the occurrence of an understory fire event, burned forests had significantly lower biomass and height than control sites. Gordon et al. [290] investigated the effect of mixed severity wildfire on the regrowth of open forests in Australia on the base of LiDAR data and field surveys. This study showed that vegetation recovery of Eucalyptus, Callitris, and Acacia species was very fragmented. The regrowth of mid-story vegetation was 22–40% lower in BA of low and moderate compared to high fire severity [290]. In order to quantify how wildfire impacts forest recovery, several researchers have examined the combined use of optical sensors imagery and LiDAR data [225,226,230,291]. Meng et al. [292] studied the recovery rate of mixed pine-oak (*Pinus rigida*) forest in Long Island (NY) three years after wildfire by leveraging 1 m of simultaneous airborne imaging spectroscopy and LiDAR and 2 m of satellite multi-spectral imagery. They presented a new method for the estimation of tree species (oak vs. pine) recovery rates to different BS levels, derived from large spatial-temporal scales. According to the study, pine trees were more resilient to high BS with a higher recovery rate (12% per year) than oak (*Quercus alba* and *Quercus coccinea*) species (4% per year) [292]. Bolton et al. [293] estimated vegetation recovery in the Canadian boreal spans following wildfire, combining LiDAR, MODIS GPP, and a national Landsat-derived record of forest change. The research showed difference in forest canopy structure across the boreal spans, while correlations to GPP were stronger for forest stands by 15–25 years post-wildfire.

Combining different RS images (optical, SAR, and LiDAR) with BS maps provides a more comprehensive assessment of post-fire forest recovery patterns. Therefore, further studies based on multi-source analysis are still needed with the inclusion of structural forest ground variables, species composition, environmental conditions, vegetation indexes, and BS [42,44,46].

4.3. Classification Algorithms

4.3.1. Feature Extraction

Choosing appropriate variables (classifiers) can be considered the crucial step for successful classification. The commonly used variables include spectral signatures, vegetation indices, transformed images, textural or contextual information, multitemporal images, multisensor im-

ages, and ancillary data [294]. Several studies used different approaches for feature extraction in BA estimations, such as the principal component model (PCA) [54,70,191,213,235,295–299], canonical correlation analysis [74,101,156,201,205,212,281,286,300–304], and multiple endmembers/spectral mixture analysis (MESMA/SMA) [37,71,86,137,154,228,231,239,289,292,305–309]. Such techniques are often used for spectral dimensionality reduction of the RS images through applying linear spectral transformations without losing important spectral features. In addition, the data compression saves further classification time, reduces the spatial noise, and provides a sharper BA signal [307].

MESMA/SMA are the most commonly used techniques for burned forests and BS detection and classification. SMA is based on modelling image spectra of the combination of particular endmembers (such as soil, forest, non-forest, etc.), and can reduce mixed pixel effects arising in the visual classification and digital processing of RS data [71,137,310]. SMA resolves the concern associated with BA that it is smaller than the pixel size of an estimated image [40,308,309]. Compared to the typical linear SMA technique, MESMA enables the use of multiple endmembers within-class spectral variability and overcomes the limitation of testing the same number of endmembers for each pixel in the image [37,239]. Many researchers used SMA/MESMA for mapping burn severity and post-fire vegetation monitoring [154,228,231,239,274,311–313].

4.3.2. Classification Methods

Since 2000, many advanced image classification methods have been developed to extract and detect the BA information from remotely sensed imagery. We summarized the classification methods into four main groups—Supervised (pixel-based and geo/object-based image analysis (GEOBIA/OBIA)), Unsupervised (pixel-based), Hybrid, Manual, and Other. The majority of remote sensing BA studies have shown preference for the supervised classification approach (82%) (Figure 8a). This is mainly because the supervised method ultimately deals with many classification algorithms, while the unsupervised method employs only a few of them, which usually have lower accuracy than the supervised methods. Several studies used supervised parametric classification algorithms such as maximum likelihood (ML) (11.3%) [53,173,210,297,314–318] and Mahalanobis distance (MD) (3.8%) [319] (Figure 8b).

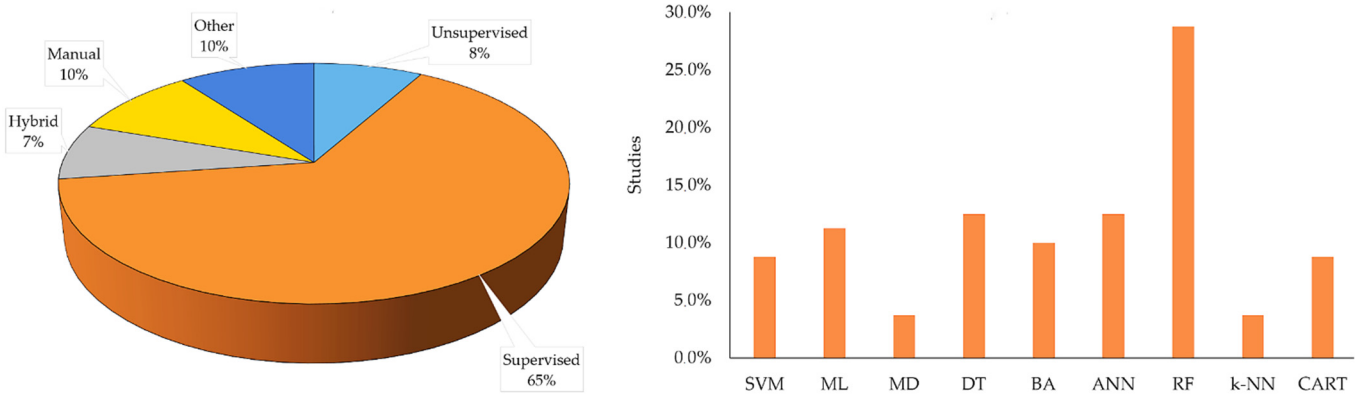

(**a**) (**b**)

Figure 8. Percentage of the studies: (**a**) classification groups, (**b**) supervised classification algorithms.

The most commonly used supervised machine learning algorithms were random forest (RF) (28.8%) [21,115–117,131,220,223,229,234,278,284,287,288,320–327], artificial neural network (ANN) (12.5%) [98,204,235,328–330], decision tree (DT) (12.5%) [27,71,108,141,321,325,331–334], Bayesian algorithm (10.0%) [87,106,112,127,198,335–337], support vector machine (SVM) (8.8%) [284,288,299,321,338,339], classification and regression tree (CART) (8.8%) [33,229,296,340–343], and k-nearest neighbour (K-NN) (3.8%) [163,235,340]. The 'Unsupervised' group of methods

included iterative self-organizing data analysis (ISODATA), self-organization cluster analysis, object-based analysis and k-means clustering [232,254,257,258,283,288,298,306,308,344–348]. The hybrid (mix of several approaches) classification was utilized in 11 of the reviewed studies [95,288,339,349].

The "Manual" group of studies were those that manually produced BA classes and BS mapping through digitizing polygons, using vegetation and spectral indices, extracting features, hotspot detection, and change analysis in forest patterns [350–366]. The burned area extraction and dating (BAED) algorithm [367], multiscale curvature classification [233], spectral angle mapper classification [155,200,317], discriminant analysis [282], and rare class prediction in the absence of true labels [368] classification methods were used less than three times, and, therefore, they were included in the "Other" group of methods.

In the last decade, the GEOBIA method has emerged based on image-objects segmentation and classification rather than pixels, which increased the land-cover studies with the use of high spatial resolution remote sensing imagery [369]. Of the total BA studies, 9% used OBIA/GEOBIA classification with the application of ground truth data and regional forest maps to validate the classification accuracy [370–372]. Application of the GEOBIA improves detection and fuzzy logic classification accuracy of BA [147,215,259,278,373,374]. In addition, the object-based approach, despite the inherent computational costs, was reported to be less time-consuming than the pixel-based approach [299]. However, pixel-based approaches are still more widely used by researchers.

4.3.3. Classification Accuracy

Several metrics such as the Kappa coefficient, overall accuracy, and omission and commission errors are typically used with the confusion matrix for burned area classification performance evaluation. A total of 151 studied papers used the error matrix method, regression analysis, and modelling for validation of BA estimation results. Table 3 summarises the distribution of the reference data type and validation methods used in these studies. Out of 151 papers, 49 (32%) used ground truth data (field survey, composite burn index, GPS points, and forest inventory sample plots) for reference purposes. From these, 20 papers provided Kappa coefficients and overall accuracy together with the error matrix results. The second group of 31 studies was based on the reference data retrieved from high resolution imagery (e.g., Google Earth, WorldView, aerial photo).

Table 3. Distribution of the reference data type and validation methods with the respective number of studies.

Reference Data	Kappa Coefficient	Omission Error	Commission Error	Overall Accuracy	R^2/RMSE	Number of Studies
Ground truth data (field survey, CBI, GPS point)	20	17	17	20	10	49
Images (Google Earth, high resolution, aerial photo)	9	8	8	10	17	31
Ancillary data (forest inventory, forest BA maps, Land use land cover)	10	9	8	9	16	37
Combination of above data	10	8	8	9	18	34
Total number of studies	49	41	49	48	61	151

Seventeen studies of this group used the coefficient of determination (R^2) with/or root mean square error (RMSE) value to describe the possible prediction accuracy of the efficient models. Thirty-seven studies used ancillary data produced by the government authorities (e.g., forest inventory maps, land use/land cover, official data of statistical agencies). In another thirty-four studies, the validation and assessment of forest BA were based on the combination of the above-mentioned reference data. For example, some studies used ground truth data and high-resolution images or ground truth data with local maps. The results in Table 3 indicate that though during the estimated 20 years the metrics of confusion matrixes were still in high demand among researchers, regression analysis and

modelling (R^2/RMSE) were the most used methods in accuracy estimation and mapping of the forest BA.

For a comprehensive analysis of the RS-based forest BA studies, the reported overall accuracies were measured and compared with several factors, such as the year of publication, classification method, respective sensor, and the reference data considered in the validation of classification results. The classification accuracy of estimates for forest BA varies significantly among the assessed studies in all four groups of factors, especially with respect to the classification accuracy of different sensors and reference data (Figure 9).

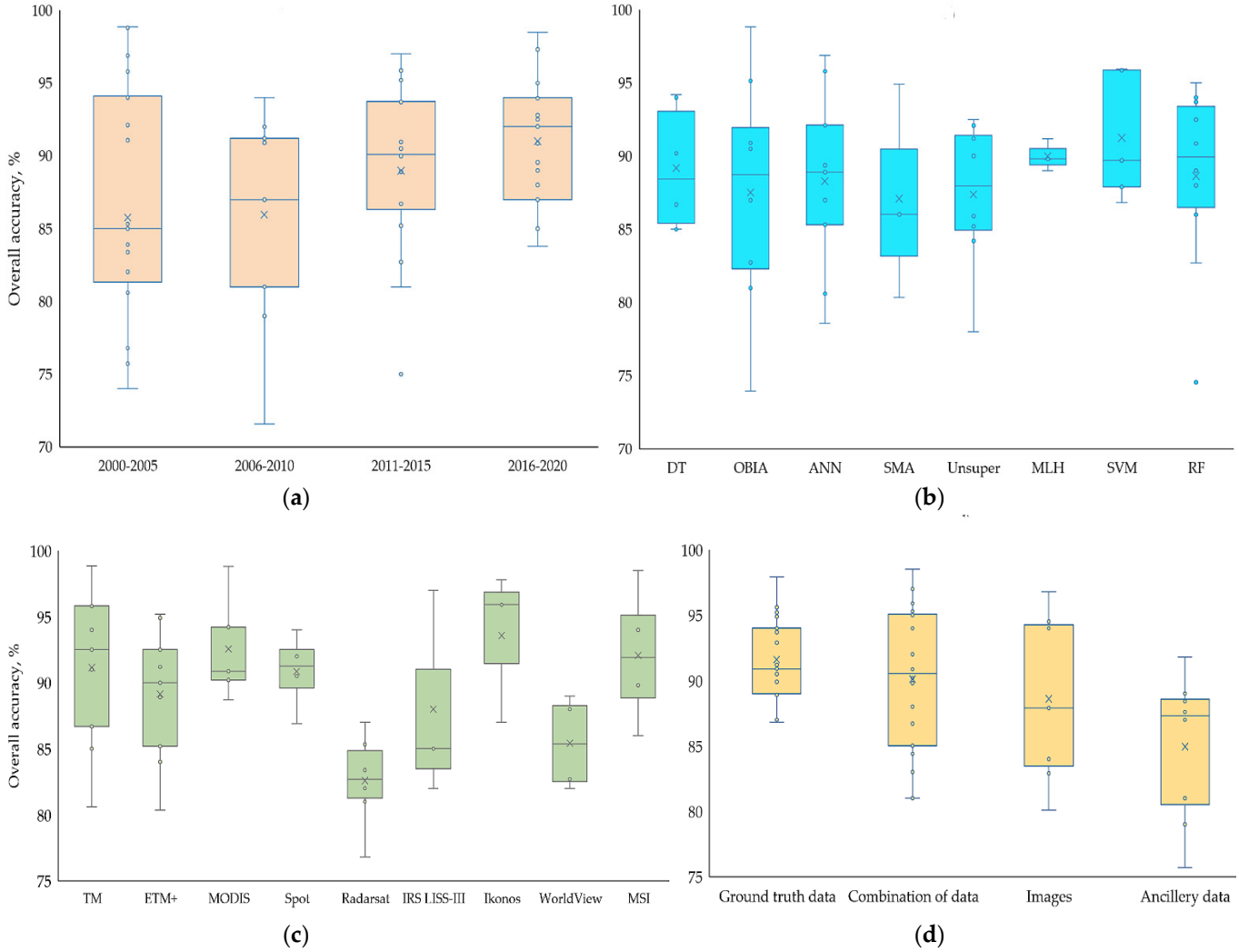

Figure 9. Overall accuracies reported in RS-based BA classification studies based on: (**a**) the year of publication, (**b**) the classification method, (**c**) the satellite sensor, and (**d**) the reference data.

From the box and whisker plots on Figure 9a, it can be seen that throughout 2000–2020, the median of overall accuracies were gradually improving. In 2000–2005, the median overall accuracies of BA classifications were about 85%, while in 2016–2020, the median increased sufficiently up to 94%. This positive tendency is likely a result of improved classification methods used in the evaluated studies, including novel classification techniques, advanced sensors, and the high quality of reference data. The most accurate results of the forest BA mapping were obtained using RF, SVM, and MLH classifiers (OA about 90%), followed by OBIA, ANN, and an unsupervised group of classifiers (OA about 88%). DT and SMA methods are characterized by a similar median classification accuracy of 85.8% and 86.4%, respectively (Figure 9b).

Figure 9c with the box and whisker plots shows the median overall accuracies of nine different sensors. It is observed that, except for RADARSAT images, the median classification accuracy is generally above 85%, with a range from 76.8% to 98.8%. IKONOS demonstrates the highest accuracy, at 95.9% median overall accuracy of BA classification, followed by Landsat TM (92.5%), SPOT (91.2%), MODIS (90.9%), and Landsat ETM+ (90.2%). Figure 9d shows that among the reference data used for validation, the median overall classification accuracy in BA studies is highest for the ground truth data and combined data, at about 90.5%. A similar median classification accuracy of 88% is also observed for ancillary data and high resolution images.

The advances in RS-based forest BA mapping methods described in the reviewed papers also leads to a great variety of overall classification accuracies. In the case of approaches using input from several factors (e.g., combination of sensors, ancillary and ground truth data), this might have the potential to improve the accuracy and interpretation of classification results. In turn, the accurate maps of BA might provide a more reliable interpretation of forest structure relative to the modelling of post-fire patterns and recovery processes.

5. Research Perspectives

The meta-analysis results provide a base for the above-mentioned challenges for future research in the field of forest BA, BS, and post-fire recovery:

- It is important to conduct more research in the forest ecosystems of South America, Africa, and Eurasia, because these regions have a great impact on the global balance of carbon and climate change.
- Further identified investigations are likely to include the use of higher resolution data, algorithms for multi-criteria analysis, empirical models, and data fusion from multiple sensors. The adoption of these methods and data can potentially address the misclassification and high variability in BA, BS, and post-fire recovery studies.
- Neural networks, classification and regression trees (CARTs), fuzzy modelling, and OBIA are also very promising in future studies with the application of big data algorithms and emerging processing platforms. The use of machine-learning algorithms and cloud computing techniques (e.g., GEE) provides a new opportunity for the field of study.
- The review suggests that more research needs to be done on finding methods for reducing RS image classification errors (omission and commission) and increasing global and regional BA map accuracy, particularly in data-poor regions.
- The combination of RS imagery from passive and active sensors can provide more insight in the field of study, including the possibility to overcome cloud cover issues in a forest BA.
- We expect to see an increase in the integration of LiDAR, radar, hyperspectral sensors, and emerging UAS technologies in future BA studies. There is also huge potential for research on the spatial and temporal pattern of post-fire recovery and approaches to forest BA monitoring with the aim of improving ecosystem sustainability.

6. Conclusions

This paper presents a comprehensive overview on the progress and development of RS-based applications in the detection and monitoring of forest burnt area. We identified a total of 329 relevant papers in a selected 48 peer-reviewed journals pertaining to all aspects of remote sensing of forest BA within the last two decades. A database containing information on RS-based forest BA estimates was constructed to serve as a base for meta-analysis. We analysed the papers with regard to the research focus, ecological zoning, spatial resolution of the RS images, temporal scope, tree species, spectral indices, reference data, overall accuracies, and classification methods applied. A deep meta-analysis was carried out to discuss the application of RS systems in forest post-fire studies worldwide, which differentiates our study from previous reviews. Topics under consideration include

burned area estimates and mapping, burn severity assessment, and monitoring of post-fire forest recovery.

Our review of the available papers indicates that the number of remote sensing studies conducted on forest BA increased substantially from the early 2000s to reach a peak in the 2011–2020 decade. The dominant studies were using optical sensors (261 cases, 80%) based on Landsat, Sentinel, Terra, Aqua, Sentinel, AVHRR, and SPOT satellites. According to the FAO Global Ecological Zone map, most of the reviewed studies were carried out within subtropical dry forest (21.4%, 92 cases). With regard to tree species discrimination, the studies mainly described pine (37.0%). The NDVI and dNBR were the most frequently used VI compared to other indices. The studies show that there are some challenges, mainly due to spectral mixing and poor validation data quality, in determining BA and BS. The use of multisensor images may improve the accuracy and reduce uncertainty in BA estimations. For instance, combining optical time series at moderate resolutions with radar data provides a good opportunity to improve the overall accuracy of the assessments. There is also a need for global and regional products with higher spatial resolution to provide the most accurate BA estimation. The use of RF, SVM, and MLH classifiers has allowed the detection of forest BA classes with no significant difference among them. During 2000–2020, classification techniques gradually tended to reach higher overall accuracies, specifically when using ground truth and combining data from different reference sources. Consequently, remote sensing is expected to improve methodologies to detect and monitor BA in a fast and cost-effective manner, and thus enhance its role in sustainable forest management.

Supplementary Materials: The analysed reference database is available online at https://www.mdpi.com/article/10.3390/rs14194714/s1, Table S1: BA supplement.

Author Contributions: Conceptualization, E.K., O.V., J.S., J.W. and J.C.; data curation, E.K., O.V., J.S. and J.W.; formal analysis, E.K., J.S., J.W. and X.L.; funding acquisition, E.K., J.S., J.W. and J.C.; investigation, E.K. and O.V.; methodology, E.K., O.V., J.S., J.W. and J.C.; project administration, E.K., J.W., J.S. and J.C.; resources, E.K., S.L., X.L., D.D. and Y.W.; software, O.V. and S.L., Y.W.; supervision, E.K., J.S. and J.W.; visualization, O.V., S.L., D.D. and Y.W.; writing—original draft, E.K., O.V., J.S., J.W. and J.C.; writing—review and editing, E.K., J.S., J.W., X.L. and J.C. All authors have read and agreed to the published version of the manuscript.

Funding: The reported study was funded by RFBR (grant No 19-55-80010/19), MOST (grant No 2018YFE0184300), and NRF (grant No 120456) according to the research project No 19-55-80010; National Natural Science Foundation of China (grant No 41961060).

Acknowledgments: This research was supported by BRICS Multilateral Joint Science and Technology Research Collaboration between Russia (Russian Foundation for Basic Research), China (National Natural Science Foundation of China), and South Africa (National Research Foundation). The authors are grateful to the three anonymous reviewers for their valuable feedback and guidance in improving the initial version of this manuscript in multiple ways.

Conflicts of Interest: The authors declare no conflict of interest.

References

1. FAO; UNEP. The State of the World's Forests 2020. In *Forests, Biodiversity and People*; FAO: Rome, Italy, 2020; p. 214.
2. Artés, T.; Oom, D.; de Rigo, D.; Durrant, T.H.; Maianti, P.; Libertà, G.; San-Miguel-Ayanz, J. A global wildfire dataset for the analysis of fire regimes and fire behaviour. *Scien. Data* **2019**, *6*, 296. [CrossRef] [PubMed]
3. FAO. *Global Forest Resources Assessment 2020: Main Report*; FAO: Rome, Italy, 2020; p. 184.
4. Ciais, P.; Sabine, C.; Bala, G.; Bopp, L.; Brovkin, V.; Canadell, J.; Chhabra, A.; DeFries, R.; Galloway, J.; Heimann, M.; et al. Carbon and other biogeochemical cycles. In *Climate Change 2013: The Physical Science Basis. Contribution of Working Group I to the Fifth Assessment Report of the Intergovernmental Panel on Climate Change*; Stocker, T.F., Qin, D., Plattner, G.-K., Tignor, M., Allen, S.K., Boschung, J., Nauels, A., Xia, Y., Bex, V., Midgley, P.M., Eds.; Cambridge University Press: Cambridge, UK, 2014; pp. 465–570.
5. Yue, C.; Ciais, P.; Cadule, P.; Thonicke, K.; van Leeuwen, T.T. Modelling the role of fires in the terrestrial carbon balance by incorporating SPITFIRE into the global vegetation model ORCHIDEE—Part 2: Carbon emissions and the role of fires in the global carbon balance. *Geosci. Model Dev.* **2015**, *8*, 1285–1297. [CrossRef]
6. Gillett, N.P.; Weaver, A.J.; Zwiers, F.W.; Flannigan, M.D. Detecting the effect of climate change on Canadian forest fires. *Geophys. Res. Lett.* **2004**, *31*, L18211. [CrossRef]

7. Crimmins, M.A. Interannual to decadal changes in extreme fire weather event frequencies across the southwestern United States. *Int. J. Climatol.* **2011**, *31*, 1573–1583. [CrossRef]
8. Drobyshev, I.; Granstrom, A.; Linderholm, H.W.; Hellberg, E.; Bergeron, Y.; Niklasson, M. Multi-century reconstruction of fire activity in Northern European boreal forest suggests differences in regional fire regimes and their sensitivity to climate. *J. Ecol.* **2014**, *102*, 738–748. [CrossRef]
9. Singleton, M.P.; Thode, A.E.; Meador, A.J.S.; Iniguez, J.M. Increasing trends in high-severity fire in the southwestern USA from 1984 to 2015. *For. Ecol. Manag.* **2019**, *433*, 709–719. [CrossRef]
10. Molina-Terren, D.M.; Xanthopoulos, G.; Diakakis, M.; Ribeiro, L.; Caballero, D.; Delogu, G.M.; Viegas, D.X.; Silva, C.A.; Cardil, A. Analysis of forest fire fatalities in Southern Europe: Spain, Portugal, Greece and Sardinia (Italy). *Int. J. Wildland Fire* **2019**, *28*, 85–98. [CrossRef]
11. Flannigan, M.D.; Stocks, B.J.; Wotton, B.M. Climate change and forest fires. *Sci. Total Environ.* **2000**, *262*, 221–229. [CrossRef]
12. Stephens, S.L.; Agee, J.K.; Fulé, P.Z.; North, M.P.; Romme, W.H.; Swetnam, T.W.; Turner, M.G. Managing forests and fire in changing climates. *Science* **2013**, *342*, 41–42. [CrossRef]
13. Etchellsa, H.; O'Donnella, A.J.; McCawb, W.L.; Griersona, P.F. Fire severity impacts on tree mortality and post-fire recruitment in tall eucalypt forests of southwest Australia. *For. Ecol. Manag.* **2020**, *459*, 117850. [CrossRef]
14. Loboda, T.; Krankina, O.; Savin, I.; Kurbanov, E.; Joanne, H. Land management and the impact of the 2010 extreme drought event on the agricultural and ecological systems of European Russia. In *Land-Cover and Land-Use Changes in Eastern Europe after the Collapse of the Soviet Union in 1991*; Gutman, G., Volker, R., Eds.; Springer International Publishing: Cham, Switzerland, 2017; pp. 173–192.
15. Seidl, R.; Schelhaas, M.J.; Rammer, W.; Verkerk, P.J. Increasing forest disturbance in Europe and their impacts on carbon storage. *Nature Clim. Change* **2014**, *4*, 806–810. [CrossRef] [PubMed]
16. Thompson, M.P.; Rodríguez y Silva, F.; Calkin, D.E.; Hand, M.S. A review of challenges to determining and demonstrating efficiency of large fire management. *Int. J. Wildland Fire* **2017**, *26*, 562–573. [CrossRef]
17. Brecka, A.F.J.; Boulanger, Y.; Searle, E.B.; Taylor, A.R.; Price, D.T.; Zhu, Y.; Shahia, C.; Chena, H.Y.H. Sustainability of Canada's forestry sector may be compromised by impending climate change. *For. Ecol. Manag.* **2020**, *474*, 118352. [CrossRef]
18. Staal, A.; van Nes, E.H.; Hantson, S.; Holmgren, M.; Dekker, S.C.; Pueyo, S.; Xu, C.; Scheffer, M. Resilience of tropical tree cover: The roles of climate, fire and herbivory. *Glob. Change Biol.* **2018**, *24*, 5096–5109. [CrossRef] [PubMed]
19. Mosquera-Losada, M.R.; Santiago-Freijanes, J.J.; Rois-Díaz, M.; Moreno, G.; den Herder, M.; Aldrey-Vázquez, J.A.; Ferreiro-Domínguez, N.; Pantera, A.; Pisanelli, A.; Rigueiro-Rodríguez, A. Agroforestry in Europe: A land management policy tool to combat climate change. *Land Use Policy* **2018**, *78*, 603–613. [CrossRef]
20. Sousa-Silva, R.; Verbist, B.; Lomba, Â.; Valent, P.; Suškevičs, M.; Picard, O.; Hoogstra-Klein, M.A.; Cosofret, V.-C.; Bouriaud, L.; Ponette, Q.; et al. Adapting forest management to climate change in Europe: Linking perceptions to adaptive responses. *For. Pol. Econ.* **2018**, *90*, 22–30. [CrossRef]
21. Otón, G.; Ramo, R.; Lizundia-Loiola, J.; Chuvieco, E. Global detection of long-term (1982–2017) burned area with AVHRR-LTDR data. *Remote Sens.* **2019**, *11*, 2079. [CrossRef]
22. Talukdar, S.; Singha, P.; Mahato, S.; Shahfahad; Pal, S.; Liou, Y.-A.; Rahman, A. Land-use land-cover classification by machine learning classifiers for satellite observations—A review. *Remote Sens.* **2020**, *12*, 1135. [CrossRef]
23. French, N.H.F.; Kasischke, E.S.; Hall, R.J.; Murphy, K.A.; Verbyla, D.L.; Hoy, E.E.; Allen, J.L. Using Landsat data to assess fire and burn severity in the North American boreal forest region: An overview and summary of results. *Int. J. Wildland Fire* **2008**, *17*, 443–462. [CrossRef]
24. Hua, L.; Shao, G. The progress of operational forest fire monitoring with infrared remote sensing. *J. For. Res.* **2017**, *28*, 215–229. [CrossRef]
25. MacDonald, H.; McKenney, D. Envisioning a global forest transition: Status, role, and implications. *Land Use Pol.* **2020**, *99*, 104808. [CrossRef]
26. Song, X.; Hansen, M.C.; Stehman, S.V.; Potapov, P.V.; Tyukavina, A.; Vermote, E.F.; Townshend, J.R. Global land change from 1982 to 2016. *Nature* **2018**, *560*, 639–643. [CrossRef]
27. Verhegghen, A.; Eva, H.; Ceccherini, G.; Achard, F.; Gond, V.; Gourlet-Fleury, S.; Cerutti, P.O. The Potential of Sentinel Satellites for Burnt Area Mapping and Monitoring in the Congo Basin Forests. *Remote Sens.* **2016**, *8*, 986. [CrossRef]
28. Santana, N.C.; De Carvalho Júnior, O.A.; Gomes, R.A.T.; Guimarães, R.F. Burned-area detection in Amazonian environments using standardized time series per pixel in MODIS data. *Remote Sens.* **2018**, *10*, 1904. [CrossRef]
29. Gupta, S.; Roy, A.; Bhavsar, D.; Kala, R.; Singh, S.; Kumar, A.S. Forest fire burnt area assessment in the biodiversity rich regions using geospatial technology: Uttarakhand forest fire event 2016. *J. Indian Soc. Remote Sens.* **2018**, *46*, 945–955. [CrossRef]
30. Campagnolo, M.L.; Oom, D.; Padilla, M.; Pereira, J.M.C. A patch-based algorithm for global and daily burned area mapping. *Rem. Sens. Environ.* **2019**, *232*, 111288. [CrossRef]
31. Roy, D.P.; Boschetti, L.; Trigg, S.N. Remote sensing of fire severity: Assessing the performance of the normalized burn ratio. *IEEE Geosci. Remote Sens. Lett.* **2006**, *3*, 112–116. [CrossRef]
32. Kurbanov, E.; Vorobyev, O.; Leznin, S.; Polevshikova, Y.; Demisheva, E. Assessment of burn severity in Middle Povozhje with Landsat multitemporal data. *Int. J. Wildland Fire* **2017**, *26*, 772–782. [CrossRef]

33. Chen, X.; Vogelmann, J.; Rollins, M.; Ohlen, D.; Key, C.; Yang, Y.; Huang, C.; Shi, H. Detecting post-fire burn severity and vegetation recovery using multitemporal remote sensing spectral indices and field-collected composite burn index data in a ponderosa pine forest. *Int. J. Remote Sens.* **2011**, *32*, 7905–7927. [CrossRef]
34. Saulino, L.; Rita, A.; Migliozzi, A.; Maffei, C.; Allevato, E.; Garonna, A.P.; Saracino, A. Detecting Burn Severity across Mediterranean Forest Types by Coupling Medium-Spatial Resolution Satellite Imagery and Field Data. *Remote Sens.* **2020**, *12*, 741. [CrossRef]
35. Cuevas-González, M.; Gerard, F.; Balzter, H.; Riano, D. Analysing forest recovery after wildfire disturbance in boreal Siberia using remotely sensed vegetation indices. *Glob. Change Biol.* **2009**, *15*, 561–577. [CrossRef]
36. Van Leeuwen, W.J.D.; Casady, G.M.; Neary, D.G.; Bautista, S.; Alloza, J.A.; Carmel, Y.; Wittenberg, L.; Malkinson, D.; Orr, B.J. Monitoring post-wildfire vegetation response with remotely sensed time-series data in Spain, USA, and Israel. *Int. J. Wildland Fire* **2010**, *19*, 75–93. [CrossRef]
37. Kibler, C.L.; Parkinson, A.-M.L.; Peterson, S.H.; Roberts, D.A.; D'Antonio, C.M.; Meerdink, S.K.; Sweeney, S.H. Monitoring post-fire recovery of chaparral and conifer species using field surveys and Landsat time series. *Remote Sens.* **2019**, *11*, 2963. [CrossRef]
38. Fernández-Guisuraga, J.M.; Suárez-Seoane, S.; Calvo, L. Transferability of vegetation recovery models based on remote sensing across different fire regimes. *Appl. Veg. Sci.* **2020**, *23*, 441–451. [CrossRef]
39. Girardin, M.P.; Ali, A.A.; Hely, C. Wildfires in boreal ecosystems: Past, present and some emerging trends. *Int. J. Wildland Fire* **2010**, *19*, 913–926. [CrossRef]
40. Gitas, I.; Mitri, G.; Veraverbeke, S.; Polychronaki, A. Advances in remote sensing of post-fire vegetation recovery monitoring—A review. In *Remote Sensing of Biomass—Principles and Applications*; Fatoyinbo, L., Ed.; InTech: London, UK, 2012; ISBN 978-953-51-0313-4.
41. Miettinen, J.; Hyer, E.; Chia, A.S.; Kwoh, L.K.; Liew, S.C. Detection of vegetation fires and burnt areas by remote sensing in insular Southeast Asian conditions: Current status of knowledge and future challenges. *Int. J. Remote Sens.* **2013**, *34*, 4344–4366. [CrossRef]
42. Chu, T.; Guo, X. Remote sensing techniques in monitoring post-fire effects and patterns of forest recovery in boreal forest regions: A review. *Remote Sens.* **2014**, *6*, 470–520. [CrossRef]
43. Parisien, M.A.; Denyse, A.D.; Miller, C.; Stockdale, C.A.; Armitage, O.B. Applications of simulation-based burn probability modelling: A review. *Int. J. Wildland Fire* **2019**, *28*, 913–926. [CrossRef]
44. Szpakowski, D.M.; Jensen, J.L.R. A Review of the applications of remote sensing in fire ecology. *Remote Sens.* **2019**, *11*, 2638. [CrossRef]
45. Liberati, A.; Altman, D.G.; Tetzlaff, J.; Mulrow, C.; Gøtzsche, P.C.; Ioannidis, J.P.A.; Clarke, M.; Devereaux, P.J.; Kleijnen, J.; Moher, D. The PRiSMA statement for reporting systematic reviews and meta-analyses of studies that evaluate healthcare interventions: Explanation and elaboration. *Res. Methods Rep.* **2009**, *62*, e1–e34. [CrossRef]
46. Chuvieco, E.; Mouillot, F.; van der Werf, G.R.; Miguel, J.S.; Tanase, M.; Koutsias, N.; García, M.; Yebra, M.; Padilla, M.; Gitas, I.; et al. Historical background and current developments for mapping burned area from satellite Earth observation. *Remote Sens. Environ.* **2019**, *225*, 45–64. [CrossRef]
47. Mouillot, F.; Schultz, M.G.; Yue, C.; Cadule, P.; Tansey, K.; Ciais, P.; Chuvieco, E. Ten years of global burned area products from spaceborne remote sensing—A review: Analysis of user needs and recommendations for future developments. *Int. J. Appl. Earth Obs. Geoinf.* **2014**, *26*, 64–79. [CrossRef]
48. Trigg, S.; Flasse, S. Characterising the spectral-temporal response of burned savanna using in situ spectroradiometry and infrared thermometry. *Int. J. Remote Sens.* **2000**, *21*, 3161–3168. [CrossRef]
49. Fraser, R.H.; Li, Z.; Cihlar, J. Hotspot and NDVI differencing synergy (HANDS): A new technique for burned area mapping over boreal forest. *Remote Sens. Environ.* **2000**, *74*, 362–376. [CrossRef]
50. Al-Rawi, K.R.; Casanova, J.L.; Romo, A.; Louakfaoui, E.M. Integrated fire evolution monitoring system (IFEMS) for monitoring spatial-temporal behaviour of multiple fire phenomena. *Int. J. Remote Sens.* **2002**, *23*, 1967–1983. [CrossRef]
51. Justice, C.O.; Smith, R.; Gill, A.M.C.I. A review of current space-based fire monitoring in Australia and the GOFC/GOLD program for international coordination. *Int. J. Wildland Fire* **2003**, *12*, 247–258. [CrossRef]
52. Li, Z.; Fraser, R.; Jin, J.; Abuelgasim, A.A.; Csiszar, I.; Gong, P.; Pu, R.; Hao, W. Evaluation of algorithms for fire detection and mapping across North America from satellite. *J. Geophys. Res. Atmos.* **2003**, *108*, 4076. [CrossRef]
53. Zhang, Y.-H.; Wooster, M.J.; Tutubalina, O.; Perry, G.L.W. Monthly burned area and forest fire carbon emission estimates for the Russian Federation from SPOT VGT. *Remote Sens. Environ.* **2003**, *87*, 1–15. [CrossRef]
54. Silva, J.M.N.; Cadima, J.F.C.L.; Pereira, J.M.C.; Grégoire, J.-M. Assessing the feasibility of a global model for multi-temporal burned area mapping using SPOT-VEGETATION data. *Int. J. Remote Sens.* **2004**, *25*, 4889–4913. [CrossRef]
55. Sukhinin, A.I.; French, N.H.F.; Kasischke, E.S.; Hewson, J.H.; Soja, A.J.; Csiszar, I.A.; Hyer, E.J.; Loboda, T.; Conard, S.G.; Romasko, V.I.; et al. AVHRR-based mapping of fires in Russia: New products for fire management and carbon cycle studies. *Remote Sens. Environ.* **2004**, *93*, 546–564. [CrossRef]
56. Kučera, J.; Yasuoka, Y.; Dye, D.G. Creating a forest fire database for the Far East of Asia using NOAA/AVHRR observation. *Int. J. Remote Sens.* **2005**, *26*, 2423–2439. [CrossRef]

57. Urbanski, S.P.; Salmon, J.M.; Nordgren, B.L.; Hao, W.M. A MODIS direct broadcast algorithm for mapping wildfire burned area in the western United States. *Remote Sens. Environ.* **2009**, *113*, 2511–2526. [CrossRef]
58. Somashekar, R.K.; Ravikumar, P.; Mohan Kumar, C.N.; Prakash, K.L.; Nagaraja, B.C. Burnt area mapping of Bandipur National Park, India using IRS 1C/1D LISS III Data. *J. Indian Soc. Remote Sens.* **2009**, *37*, 37–50. [CrossRef]
59. Merino-de-Miguel, S.; Huesca, M.; González-Alonso, F. Modis reflectance and active fire data for burn mapping and assessment at regional level. *Ecol. Model.* **2010**, *221*, 67–74. [CrossRef]
60. Libonati, R.; DaCamara, C.C.; Pereira, J.M.C.; Peres, L.F. Retrieving middle-infrared reflectance for burned area mapping in tropical environments using MODIS. *Remote Sens. Environ.* **2010**, *114*, 831–843. [CrossRef]
61. Badarinath, K.V.S.; Sharma, A.R.; Kharol, S.K. Forest fire monitoring and burnt area mapping using satellite data: A study over the forest region of Kerala state, India. *Int. J. Remote Sens.* **2011**, *32*, 85–102. [CrossRef]
62. Stroppiana, D.; Bordogna, G.; Carrara, P.; Boschetti, M.; Boschetti, L.; Brivio, P. A method for extracting burned areas from Landsat TM/ETM+ images by soft aggregation of multiple Spectral Indices and a region growing algorithm. *ISPRS J. Photogramm. Remote Sens.* **2012**, *69*, 88–102. [CrossRef]
63. Briones-Herrera, C.I.; Vega-Nieva, D.J.; Monjarás-Vega, N.A.; Briseño-Reyes, J.; López-Serrano, P.M.; Corral-Rivas, J.J.; Alvarado-Celestino, E.; Arellano-Pérez, S.; Álvarez-González, J.G.; Ruiz-González, A.D.; et al. Near real-time automated early mapping of the perimeter of large forest fires from the aggregation of VIIRS and MODIS active fires in Mexico. *Remote Sens.* **2020**, *12*, 2061. [CrossRef]
64. Santos, F.L.M.; Libonati, R.; Peres, L.F.; Pereira, A.A.; Narcizo, L.C.; Rodrigues, J.A.; Oom, D.; Pereira, J.M.C.; Schroeder, W.; Setzer, A.W. Assessing VIIRS capabilities to improve burned area mapping over the Brazilian Cerrado. *Int. J. Remote Sens.* **2020**, *41*, 8300–8327. [CrossRef]
65. Li, Z.; Cihlar, J.; Nadon, S.; Stocks, B. Satellite-based mapping of Canadian Boreal forest fires: Evaluation and comparison of algorithms. *Int. J. Remote Sens.* **2000**, *21*, 3071–3082. [CrossRef]
66. Cochrane, M.A.; Laurance, W.F. Fire as a large-scale edge effect in Amazonian forests. *J. Trop. Ecol.* **2002**, *18*, 311–325. [CrossRef]
67. Gerard, F.; Plummer, S.; Wadsworth, R.; Ferreruela, A.; Iliffe, L.; Balzter, H.; Wyatt, B. Forest fire scar detection in the boreal forest with multitemporal SPOT-VEGETATION Data. *IEEE Trans. Geosci. Remote Sens.* **2003**, *41*, 2575–2585. [CrossRef]
68. Koutsias, N.; Pleniou, M. Comparing the spectral signal of burned surfaces between Landsat 7 ETM+ and Landsat 8 OLI sensors. *Int. J. Remote Sens.* **2015**, *36*, 3714–3732. [CrossRef]
69. Vázquez, A.; Cuevas, J.M.; González-Alonso, F. Comparison of the use of WiFS and LISS images to estimate the area burned in a large forest fire. *Int. J. Remote Sens.* **2001**, *22*, 901–907. [CrossRef]
70. Salvador, R.; Valeriano, J.; Pons, X.; Diaz-Delgado, R. A semi-automatic methodology to detect fire scars in shrubs and evergreen forests with Landsat MSS time series. *Int. J. Remote Sens.* **2000**, *21*, 655–671. [CrossRef]
71. Rogan, J.; Franklin, J. Mapping wildfire burn severity in Southern California forests and shrublands using enhanced thematic mapper imagery. *Geocarto Int.* **2001**, *16*, 91–106. [CrossRef]
72. Domenikiotis, C.; Dalezios, N.R.; Loukas, A.; Karteris, M. Agreement assessment of NOAA/AVHRR NDVI with Landsat TM NDVI for mapping burned forested areas. *Int. J. Remote Sens.* **2002**, *23*, 4235–4246. [CrossRef]
73. Bucini, G.; Lambin, E.F. Fire impacts on vegetation in Central Africa: A remote-sensing-based statistical analysis. *Appl. Geogr.* **2002**, *22*, 27–48. [CrossRef]
74. Isaev, A.S.; Korovin, G.N.; Bartalev, S.A.; Ershov, D.V.; Janetos, A.; Kasischke, E.S.; Shugart, H.H.; French, N.H.F.; Orlick, B.E.; Murphy, T.L. Using remote sensing to assess Russian forest fire carbon emissions. *Clim. Change* **2002**, *55*, 235–249. [CrossRef]
75. Phulpin, T.; Lavenu, F.; Bellan, M.F.; Mougenot, B.; Blasco, F. Using SPOT-4 HRVIR and VEGETATION sensors to assess impact of tropical forest fires in Roraima, Brazil. *Int. J. Remote Sens.* **2002**, *23*, 1943–1966. [CrossRef]
76. Lloret, F.; Calvo, E.; Pons, X.; Díaz-Delgado, R. Wildfires and landscape patterns in the Eastern Iberian Peninsula. *Landsc. Ecol.* **2002**, *17*, 745–759. [CrossRef]
77. Silva, J.M.N.; José, M.C.; Pereira, J.M.C.; Cabral, A.I.; Sá, A.C.L.; Vasconcelos, M.J.P.; Mota, B.; Grégoire, J.M. An estimate of the area burned in southern Africa during the 2000 dry season using SPOT-VEGETATION satellite data. *J. Geophys. Res. Atmos.* **2003**, *108*, 8498. [CrossRef]
78. Sa, A.C.L.; Pereira, J.M.C.; Vasconcelos, M.J.P.; Silva, J.M.N.; Ribeiro, N.; Awasse, A. Assessing the feasibility of sub-pixel burned area mapping in miombo woodlands of northern Mozambique using MODIS imagery. *Int. J. Remote Sens.* **2003**, *24*, 1783–1796. [CrossRef]
79. Alcaraz-Segura, D.; Chuvieco, E.; Epstein, H.E.; Kasischke, E.S.; Trishchenko, A. Debating the greening vs. browning of the North American boreal forest: Differences between satellite datasets. *Glob. Change Biol.* **2010**, *16*, 760–770. [CrossRef]
80. Ardakani, A.S.; Valadan Zoej, M.J.; Mohammadzadeh, A.; Mansourian, A. Spatial and temporal analysis of fires detected by MODIS data in Northern Iran from 2001 to 2008. *IEEE J. Sel. Top. Appl. Earth Obs. Remote Sens.* **2011**, *4*, 216–225. [CrossRef]
81. Vilar, L.; Camia, A.; San-Miguel-Ayanz, J. A comparison of remote sensing products and forest fire statistics for improving fire information in Mediterranean Europe. *Eur. J. Remote Sens.* **2015**, *48*, 345–364. [CrossRef]
82. Belhadj-Khedher, C.; Koutsias, N.; Karamitsou, A.; EI-Melki, T.; Ouelhazi, B.; Hamdi, A.; Nouri, H.; Mouillot, F. A revised historical fire regime analysis in Tunisia (1985–2010) from a critical analysis of the National fire database and remote sensing. *Forests* **2018**, *9*, 59. [CrossRef]

83. Bentekhici, N.; Bellal, S.A.; Zegrar, A. Contribution of remote sensing and GIS to mapping the fire risk of Mediterranean forest case of the forest massif of Tlemcen (North-West Algeria). *Nat. Hazards* **2020**, *104*, 811–831. [CrossRef]
84. Pinty, B.; Verstraete, M.M. GEMI: A non-linear index to monitor global vegetation from satellites. *Vegetatio* **1992**, *101*, 15–20. [CrossRef]
85. Chuvieco, E.; Englefield, P.; Trishchenko, A.P.; Luo, Y. Generation of long time series of burn area maps of the boreal forest from NOAA—AVHRR composite data. *Remote Sens. Environ.* **2008**, *112*, 2381–2396. [CrossRef]
86. Matricardi, E.A.T.; Skole, D.L.; Pedlowski, M.A.; Chomentowski, W. Assessment of forest disturbances by selective logging and forest fires in the Brazilian Amazon using Landsat data. *Int. J. Remote Sens.* **2013**, *34*, 1057–1086. [CrossRef]
87. Guindos-Rojas, F.; Arbelo, M.; García-Lázaro, J.R.; Moreno-Ruiz, J.A.; Hernández-Leal, P.A. Evaluation of a Bayesian algorithm to detect burned areas in the Canary Islands' dry woodlands and forests ecoregion using MODIS data. *Remote Sens.* **2018**, *10*, 789. [CrossRef]
88. Chuvieco, E.; Martín, M.P.; Palacios, A. Assessment of different spectral indexes in the red-near-infrared spectral domain for burned land discrimination. *Int. J. Remote Sens.* **2002**, *23*, 5103–5110. [CrossRef]
89. Martín, M.P.; Gómez, I.; Chuvieco, E. Burnt Area Index (BAIM) for burned area discrimination at regional scale using MODIS data. *For. Ecol. Manag.* **2006**, *234*, S221. [CrossRef]
90. Gonzalez-Alonso, F.; Merino-De-Miguel, S. Integration of AWiFS and MODIS active fire data for burn mapping at regional level using the Burned Area Synergic Algorithm (BASA). *Int. J. Wildland Fire* **2009**, *18*, 404–414. [CrossRef]
91. Quintano, C.; Fernández-Manso, A.; Stein, A.; Bijker, W. Estimation of area burned by forest fires in Mediterranean countries: A remote sensing data mining perspective. *For. Ecol. Manag.* **2011**, *262*, 1597–1607. [CrossRef]
92. Trigg, S.; Flasse, S. An evaluation of different bi-spectral spaces for discriminating burned shrub-savannah. *Int. J. Remote Sens.* **2001**, *22*, 2641–2647. [CrossRef]
93. Barboza Castillo, E.; Turpo Cayo, E.Y.; de Almeida, C.M.; Salas López, R.; Rojas Briceño, N.B.; Silva López, J.O.; Barrena Gurbillón, M.Á.; Oliva, M.; Espinoza-Villar, R. Monitoring Wildfires in the Northeastern Peruvian Amazon Using Landsat-8 and Sentinel-2 Imagery in the GEE Platform. *ISPRS Int. J. Geo-Inf.* **2020**, *9*, 564. [CrossRef]
94. Hawbaker, T.J.; Vanderhoof, M.K.; Schmidt, G.L.; Beal, Y.-J.; Picotte, J.J.; Takacs, J.D.; Falgout, J.T.; Dwyer, J.L. The Landsat burned area algorithm and products for the conterminous United States. *Remote Sens. Environ.* **2020**, *244*, 111801. [CrossRef]
95. Bastarrika, A.; Chuvieco, E.; Martín, M.P. Mapping burned areas from Landsat TM/ETM+ data with a two-phase algorithm: Balancing omission and commission errors. *Remote Sens. Environ.* **2011**, *115*, 1003–1012. [CrossRef]
96. Tansey, K.; Grégoire, J.-M.; Binaghi, E.; Boschetti, L.; Brivio, P.; Ershov, D.; Flasse, S.; Frazer, R.; Graetz, D.; Maggi, M.; et al. A global inventory of burned areas at 1 km resolution for the year 2000 derived from SPOT vegetation data. *Clim. Change* **2004**, *67*, 345–377. [CrossRef]
97. Tansey, K.; Grégoire, J.-M.; Defourny, P.; Leigh, R.; Pekel, J.-F.; van Bogaert, E.; Bartholomé, E. A new, global, multi-annual (2000–2007) burnt area product at 1 km resolution. *Geophys. Res. Lett.* **2008**, *35*, L01401. [CrossRef]
98. Fraser, R.H.; Li, Z. Estimating fire-related parameters in boreal forest using SPOT VEGETATION. *Remote Sens. Environ.* **2002**, *82*, 95–110. [CrossRef]
99. Simon, M.; Plummer, S.; Fierens, F.; Hoelzemann, J.J.; Arino, O. Burnt area detection at global scale using ATSR-2: The GLOBSCAR products and their qualification. *J. Geophys. Res.* **2004**, *109*, D14S02. [CrossRef]
100. Plummer, S.; Olivier, A.; Muriel, S.; Will, S. Establishing a Earth observation product service for the terrestrial carbon community: The globcarbon initiative. *Mitig. Adap. Strat. Glob. Change* **2006**, *11*, 97–111. [CrossRef]
101. Roy, D.P.; Jin, Y.; Lewis, P.E.; Justice, C.O. Prototyping a global algorithm for systematic fire-affected area mapping using MODIS time series data. *Remote Sens. Environ.* **2005**, *97*, 137–162. [CrossRef]
102. Giglio, L.; Loboda, T.; Roy, D.P.; Quayle, B.; Justice, C.O. An active-fire based burned area mapping algorithm for the MODIS sensor. *Remote Sens. Environ.* **2009**, *113*, 408–420. [CrossRef]
103. Roy, D.P.; Boschetti, L.; Justice, C.O.; Ju, J. The collection 5 MODIS burned area product—Global evaluation by comparison with the MODIS active fire product. *Remote Sens. Environ.* **2008**, *112*, 3690–3707. [CrossRef]
104. Boschetti, L.; Roy, D.; Barbosa, P.; Boca, R.; Justice, C. A MODIS assessment of the summer 2007 extent burned in Greece. *Int. J. Remote Sens.* **2008**, *29*, 2433–2436. [CrossRef]
105. Loboda, T.V.; Hoy, E.E.; Giglio, L.; Kasischke, E.S. Mapping burned area in Alaska using MODIS data: A data limitations-driven modification to the regional burned area algorithm. *Int. J. Wildland Fire* **2011**, *20*, 487–496. [CrossRef]
106. Ruiz, J.A.M.; Lázaro, J.R.G.; Cano, I.D.A.; Leal, P.H. Burned area mapping in the North American boreal forest using terra-MODIS LTDR (2001–2011): A comparison with the MCD45A1, MCD64A1 and BA GEOLAND-2 products. *Remote Sens.* **2013**, *6*, 815–840. [CrossRef]
107. Libonati, R.; DaCamara, C.C.; Setzer, A.W.; Morelli, F.; Melchiori, A.E. An algorithm for burned area detection in the Brazilian Cerrado using 4 μm MODIS imagery. *Remote Sens.* **2015**, *7*, 15782–15803. [CrossRef]
108. Chen, J.; Sheng, S.; Liu, Z. Detection of annual burned forest area using change metrics constructed from MODIS data in Manitoba, Canada. *Int. J. Remote Sens.* **2015**, *36*, 3913–3931. [CrossRef]
109. Chen, D.; Pereira, J.M.C.; Masiero, A.; Pirotti, F. Mapping fire regimes in China using MODIS active fire and burned area data. *Appl. Geogr.* **2017**, *85*, 14–26. [CrossRef]

110. Giglio, L.; Boschetti, L.; Roy, D.P.; Humber, M.L.; Justice, C.O. The collection 6 MODIS burned area mapping algorithm and product. *Remote Sens. Environ.* **2018**, *217*, 72–85. [CrossRef]
111. Moreno-Ruiz, J.A.; García-Lázaro, J.R.; Arbelo, M.; Riaño, D. A comparison of burned area time series in the Alaskan boreal forests from different remote sensing products. *Forests* **2019**, *10*, 363. [CrossRef]
112. García-Lázaro, J.R.; Ruiz, J.A.M.; Riaño, D.; Arbelo, M. Estimation of burned area in the northeastern Siberian boreal forest from a long-term data record (LTDR) 1982–2015 time series. *Remote Sens.* **2018**, *10*, 940. [CrossRef]
113. Davies, D.K.; Ilavajhala, S.; Wong, M.M.; Justice, C.O. Fire information for resource management system: Archiving and distributing MODIS active fire data. *IEEE Trans. Geosci. Remote.* **2009**, *47*, 72–79. [CrossRef]
114. Reddy, C.S.; Bird, N.G.; Sreelakshmi, S.; Manikandan, T.M.; Asra, M.; Krishna, P.H.; Jha, C.S.; Rao, P.V.N.; Diwakar, P.G. Identification and characterization of spatio-temporal hotspots of forest fires in South Asia. *Environ. Monit. Assess.* **2019**, *191*, 791. [CrossRef]
115. Chuvieco, E.; Lizundia-Loiola, J.; Pettinari, M.L.; Ramo, R.; Padilla, M.; Tansey, K.; Mouillot, F.; Laurent, P.; Storm, T.; Heil, A.; et al. Generation and analysis of a new global burned area product based on Modis 250 m reflectance bands and thermal anomalies. *Earth Syst. Sci. Data.* **2018**, *10*, 2015–2031. [CrossRef]
116. Long, T.; Zhang, Z.; He, G.; Jiao, W.; Tang, C.; Wu, B.; Zhang, X.; Wang, G.; Yin, R. 30 m resolution Global Annual Burned Area Mapping Based on Landsat images and Google Earth Engine. *Remote Sens.* **2019**, *11*, 489. [CrossRef]
117. Zhang, Z.; Long, T.; He, G.; Wei, M.; Tang, C.; Wang, W.; Wang, G.; She, W.; Zhang, X. Study on Global burned forest areas based on Landsat data. *Photogramm. Eng. Remote Sens.* **2020**, *86*, 503–508. [CrossRef]
118. Roteta, E.; Bastarrika, A.; Ibisate, A.; Chuvieco, E. A Preliminary Global Automatic Burned-Area Algorithm at Medium Resolution in Google Earth Engine. *Remote Sens.* **2021**, *13*, 4298. [CrossRef]
119. Chuvieco, E.; Opazo, S.; Sione, W.; Valle, H.D.; Anaya, J.; Di Bella, C.; Cruz, I.; Manzo, L.; Lopez, G.; Mari, N.; et al. Global burned-land estimation in Latin America using MODIS composite data. *Ecol. Appl.* **2008**, *18*, 64–79. [CrossRef] [PubMed]
120. Boschetti, L.; Roy, D.P.; Giglio, L.; Huang, H.; Zubkova, M.; Humber, M.L. Global validation of the collection 6 MODIS burned area product. *Remote Sens. Environ.* **2019**, *235*, 111490. [CrossRef]
121. Oliva, P.; Schroeder, W. Assessment of VIIRS 375 m active fire detection product for direct burned area mapping. *Remote Sens. Environ.* **2015**, *160*, 144–155. [CrossRef]
122. Olofsson, P.; Foody, G.M.; Herold, M.; Stehman, S.V.; Woodcock, C.E.; Wulder, M.A. Good practices for estimating area and assessing accuracy of land change. *Remote Sens. Environ.* **2014**, *148*, 42–57. [CrossRef]
123. Boschetti, L.; Stehman, S.V.; Roy, D.P. A stratified random sampling design in space and time for regional to global scale burned area product validation. *Remote Sens. Environ.* **2016**, *186*, 465–478. [CrossRef]
124. Padilla, M.; Olofsson, P.; Stehman, S.V.; Tansey, K.; Chuvieco, E. Stratification and sample allocation for reference burned area data. *Remote Sens. Environ.* **2017**, *203*, 240–255. [CrossRef]
125. Bourgeau-Chavez, L.L.; Kasischke, E.S.; Brunzell, S.; Mudd, J.P.; Tukman, M. Mapping fire scars in global boreal forests using imaging radar data. *Int. J. Remote Sens.* **2002**, *23*, 4211–4234. [CrossRef]
126. Tansey, K.; Gre´goire, J.-M.; Stroppiana, D.; Sousa, A.; Silva, J.; Pereira, J.M.C.; Boschetti, L.; Maggi, M.; Brivio, P.A.; Fraser, R.; et al. Vegetation burning in the year 2000: Global burned area estimates from SPOT VEGETATION data. *J. Geophys. Res. D Atmos.* **2004**, *109*, D14S03. [CrossRef]
127. Ruiz, J.A.M.; Riaño, D.; Arbelo, M.; French, N.H.F.; Ustin, S.L.; Whiting, M.L. Burned area mapping time series in Canada (1984–1999) from NOAA-AVHRR LTDR: A comparison with other remote sensing products and fire perimeters. *Remote Sens. Environ.* **2012**, *117*, 407–414. [CrossRef]
128. Fornacca, D.; Ren, G.; Xiao, W. Performance of three MODIS Fire products (MCD45A1, MCD64A1, MCD14ML), and ESA Fire_CCI in a mountainous area of Northwest Yunnan, China, characterized by frequent small fires. *Remote Sens.* **2017**, *9*, 1131. [CrossRef]
129. Humber, M.L.; Boschetti, L.; Giglio, L.; Justice, C.O. Spatial and temporal intercomparison of four global burned area products. *Int. J. Digit. Earth* **2018**, *12*, 460–484. [CrossRef] [PubMed]
130. Lizundia-Loiola, J.; Pettinari, M.L.; Chuvieco, E. Temporal anomalies in burned area trends: Satellite estimations of the Amazonian 2019 fire crisis. *Remote Sens.* **2020**, *12*, 151. [CrossRef]
131. Tanase, M.A.; Belenguer-Plomer, M.A.; Roteta, E.; Bastarrika, A.; Wheeler, J.; Fernández-Carrillo, Á.; Tansey, K.; Wiedemann, W.; Navratil, P.; Lohberger, S.; et al. Burned area detection and mapping: Intercomparison of Sentinel-1 and Sentinel-2 based algorithms over tropical Africa. *Remote Sens.* **2020**, *12*, 334. [CrossRef]
132. Padilla, M.; Stehman, S.V.; Ramo, R.; Corti, D.; Hantson, S.; Oliva, P.; Alonso-Canas, I.; Bradley, A.V.; Tansey, K.; Mota, B.; et al. Comparing the accuracies of remote sensing global burned area products using stratified random sampling and estimation. *Remote Sens. Environ.* **2015**, *160*, 114–121. [CrossRef]
133. Pessôa, A.C.M.; Anderson, L.O.; Carvalho, N.S.; Campanharo, W.A.; Junior, C.H.L.S.; Rosan, T.M.; Reis, J.B.C.; Pereira, F.R.S.; Assis, M.; Jacon, A.D.; et al. Intercomparison of burned area products and its implication for carbon emission estimations in the Amazon. *Remote Sens.* **2020**, *12*, 3864. [CrossRef]
134. Key, C.H.; Benson, N.C. Landscape Assessment (LA). In *FIREMON Fire Effects Monitoring and Inventory System*; Gen Tech Rep RMRS-GTR-164-CD; Lutes, D.C., Keane, R.E., Caratti, J.F., Key, C.H., Benson, N.C., Sutherl, S., Gangi, L.J., Eds.; Department of Agriculture, Forest Service, Rocky Mountain Research Station: Fort Collins, CO, USA, 2006; Volume 164, p. LA-1-55.

135. Lentile, L.B.; Holden, Z.A.; Smith, A.M.S.; Falkowski, M.J.; Hudak, A.T.; Morgan, P.; Lewis, S.A.; Gessler, P.E.; Benson, N.C. Remote sensing techniques to assess active fire characteristics and post-fire effects. *Int. J. Wildland Fire* **2006**, *15*, 319–345. [CrossRef]
136. Barrett, K.; Kasischke, E.S.; McGuire, A.D.; Turetsky, M.R.; Kane, E.S. Modeling fire severity in black spruce stands in the Alaskan boreal forest using spectral and non-spectral geospatial data. *Remote Sens. Environ.* **2010**, *114*, 1494–1503. [CrossRef]
137. Robichaud, P.R.; Lewis, S.A.; Laes, D.Y.M.; Hudad, A.T.; Kokaly, R.F.; Zamudio, J.A. Post-fire soil burn severity mapping with hyperspectral image unmixing. *Remote Sens. Environ.* **2007**, *108*, 467–480. [CrossRef]
138. Sobrino, J.; Llorens, R.; Fernández, C.; Fernández-Alonso, J.; Vega, J. Relationship between soil burn severity in forest fires measured in situ and through spectral indices of remote detection. *Forests* **2019**, *10*, 457. [CrossRef]
139. Kasischke, E.S.; Turetsky, M.R.; Ottmar, R.D.; French, N.H.F.; Hoy, E.E.; Kane, E.S. Evaluation of the composite burn index for assessing fire severity in Alaskan black spruce forests. *Int. J. Wildland Fire* **2008**, *17*, 515–526. [CrossRef]
140. Holden, Z.A.; Morgan, P.; Crimmins, M.A.; Steinhorst, R.K.; Smith, A.M.S. Fire season precipitation variability influences fire extent and severity in a large southwestern wilderness area, United States. *Geophys. Res. Lett.* **2007**, *34*, L16708. [CrossRef]
141. Wylie, B.K.; Zhang, L.; Bliss, N.; Ji, L.; Tieszen, L.L.; Jolly, W.M. Integrating modelling and remote sensing to identify ecosystem performance anomalies in the boreal forest, Yukon river basin, Alaska. *Int. J. Digit. Earth* **2008**, *1*, 196–220. [CrossRef]
142. Picotte, J.J.; Robertson, K.M. Validation of remote sensing of burn severity in south-eastern US ecosystems. *Int. J. Wildland Fire* **2011**, *20*, 453–464. [CrossRef]
143. Tanase, M.A.; Kennedy, R.; Aponte, C. Fire severity estimation from space: A comparison of active and passive sensors and their synergy for different forest types. *Int. J. Wildland Fire* **2015**, *24*, 1062–1075. [CrossRef]
144. Quintano, C.; Fernández-Manso, A.; Calvo, L.; Marcos, E.; Valbuena, L. Land surface temperature as potential indicator of burn severity in forest Mediterranean ecosystems. *Int. J. Appl. Earth Obs. Geoinf.* **2015**, *36*, 1–12. [CrossRef]
145. Chang, Y.; Zhu, Z.; Feng, Y.; Li, Y.; Bu, R.; Hu, Y. The spatial variation in forest burn severity in Heilongjiang Province, China. *Nat. Hazards* **2016**, *81*, 981–1001. [CrossRef]
146. Zheng, Z.; Zeng, Y.; Li, S.; Huang, W. A new burn severity index based on land surface temperature and enhanced vegetation index. *Int. J. Appl. Earth Obs. Geoinf.* **2016**, *45*, 84–94. [CrossRef]
147. Dragozi, E.; Gitas, I.Z.; Bajocco, S.; Stavrakoudis, D.G. Exploring the relationship between burn severity field data and very high resolution GeoEye images: The Case of the 2011 Evros wildfire in Greece. *Remote Sens.* **2016**, *8*, 566. [CrossRef]
148. Warner, T.A.; Skowronski, N.S.; Gallagher, M.R. High spatial resolution burn severity mapping of the New Jersey Pine Barrens with WorldView-3 near-infrared and shortwave infrared imagery. *Int. J. Remote Sens.* **2017**, *38*, 598–616. [CrossRef]
149. Addison, P.; Oommen, T. Utilizing satellite radar remote sensing for burn severity estimation. *Int. J. Appl. Earth Obs. Geoinf.* **2018**, *73*, 292–299. [CrossRef]
150. Michael, Y.; Lensky, I.M.; Brenner, S.; Tchetchik, A.; Tessler, N.; Helman, D. Economic assessment of fire damage to urban forest in the wildland–urban interface using Planet Satellites constellation images. *Remote Sens.* **2018**, *10*, 1479. [CrossRef]
151. Nigro, K.; Molinari, N. Status and trends of fire activity in southern California yellow pine and mixed conifer forests. *For. Ecol. Manag.* **2019**, *441*, 20–31. [CrossRef]
152. Quintano, C.; Fernandez-Manso, A.; Marcos, E.; Calvo, L. Burn severity and post-fire land surface albedo relationship in Mediterranean forest ecosystems. *Remote Sens.* **2019**, *11*, 2309. [CrossRef]
153. Xu, W.; He, H.S.; Hawbaker, T.J.; Zhu, Z.; Henne, P.D. Estimating burn severity and carbon emissions from a historic megafire in boreal forests of China. *Sci. Total Environ.* **2020**, *716*, 136534. [CrossRef]
154. Fernández-Guisuraga, J.M.; Calvo, L.; Suárez-Seoane, S. Comparison of pixel unmixing models in the evaluation of post-fire forest resilience based on temporal series of satellite imagery at moderate and very high spatial resolution. *ISPRS J. Photogramm. Remote Sens.* **2020**, *164*, 217–228. [CrossRef]
155. De Santis, A.; Chuvieco, E. Burn severity estimation from remotely sensed data: Performance of simulation versus empirical models. *Remote Sens. Environ.* **2007**, *108*, 422–435. [CrossRef]
156. De Santis, A.; Chuvieco, E. GeoCBI: A modified version of the Composite Burn Index for the initial assessment of the short-term burn severity from remotely sensed data. *Remote Sens. Environ.* **2009**, *113*, 554–562. [CrossRef]
157. De Santis, A.; Asner, G.P.; Vaughan, P.J.; Knapp, D.E. Mapping burn severity and burning efficiency in California using simulation models and Landsat imagery. *Remote Sens. Environ.* **2010**, *114*, 1535–1545. [CrossRef]
158. Veraverbeke, S.; Lhermitte, S.; Verstraeten, W.; Goossens, R. A time-integrated MODIS burn severity assessment using the multi-temporal differenced normalized burn ratio (dNBRMT). *Int. J. Appl. Earth Obs. Geoinf.* **2011**, *13*, 52–58. [CrossRef]
159. de la Barrera, F.; Barraza, F.; Favier, P.; Ruiz, V.; Quense, J. Megafires in Chile 2017: Monitoring multiscale environmental impacts of burned ecosystems. *Sci. Total Environ.* **2018**, *637*, 1526–1536. [CrossRef] [PubMed]
160. He, Y.; Chen, G.; De Santis, A.; Roberts, D.A.; Zhou, Y.; Meentemeyer, R.K. A disturbance weighting analysis model (DWAM) for mapping wildfire burn severity in the presence of forest disease. *Remote Sens. Environ.* **2019**, *221*, 108–121. [CrossRef]
161. Boer, M.M.; Macfarlane, C.; Norris, J.; Sadler, R.J.; Wallace, J.; Grierson, P.F. Mapping burned areas and burn severity patterns in SW Australian eucalypt forest using remotely-sensed changes in leaf area index. *Remote Sens. Environ.* **2008**, *112*, 4358–4369. [CrossRef]
162. Franks, S.; Masek, J.G.; Turner, M.G. Monitoring forest regrowth following large scale fire using satellite data: A case study of Yellowstone National Park, USA. *Eur. J. Remote Sens.* **2013**, *46*, 561–569. [CrossRef]

163. de Almeida, D.R.A.; Nelson, B.W.; Schietti, J.; Gorgens, E.B.; Resende, A.F.; Stark, S.C.; Valbuena, R. Contrasting fire damage and fire susceptibility between seasonally flooded forest and upland forest in the Central Amazon using portable profiling LiDAR. *Remote Sens. Environ.* **2016**, *184*, 153–160. [CrossRef]
164. Filipponi, F. Exploitation of Sentinel-2 time series to map burned areas at the national level: A case study on the 2017 Italy wildfires. *Remote Sens.* **2019**, *11*, 622. [CrossRef]
165. French, N.H.F.; Graham, J.; Whitman, E.; Bourgeau-Chavez, L.L. Quantifying surface severity of the 2014 and 2015 fires in the Great Slave Lake area of Canada. *Int. J. Wildland Fire* **2020**, *29*, 892–906. [CrossRef]
166. Zheng, Z.; Wang, J.; Shan, B.; He, Y.; Liao, C.; Gao, Y.; Yang, S. A new model for transfer learning-based mapping of burn severity. *Remote Sens.* **2020**, *12*, 708. [CrossRef]
167. Soverel, N.O.; Perrakis, D.D.B.; Coops, N.C. Estimating burn severity from Landsat dNBR and RdNBR indices across western Canada. *Remote Sens. Environ.* **2010**, *114*, 1896–1909. [CrossRef]
168. Hall, R.J.; Freeburn, J.T.; de Groot, W.J.; Pritchard, J.M.; Lynham, T.J.; Landry, R. Remote sensing of burn severity: Experience from western Canada boreal fires. *Int. J. Wildland Fire* **2008**, *17*, 476–489. [CrossRef]
169. Ireland, G.; Petropoulos, G.P. Exploring the relationships between post-fire vegetation regeneration dynamics, topography and burn severity: A case study from the Montane Cordillera Ecozones of Western Canada. *Appl. Geogr.* **2015**, *56*, 232–248. [CrossRef]
170. Tran, B.N.; Tanase, M.A.; Bennett, L.T.; Aponte, C. Evaluation of spectral indices for assessing fire severity in Australian temperate forests. *Remote Sens.* **2018**, *10*, 1680. [CrossRef]
171. Ressl, R.; Lopez, G.; Cruz, I.; Colditz, R.R.; Schmidt, M.; Ressl, S.; Jiménez, R. Operational active fire mapping and burnt area identification applicable to Mexican Nature Protection Areas using MODIS and NOAA-AVHRR direct readout data. *Remote Sens. Environ.* **2009**, *113*, 1113–1126. [CrossRef]
172. Cocke, A.E.; Fulé, P.Z.; Crouse, J.E. Comparison of burn severity assessments using Differenced Normalized Burn Ratio and ground data. *Int. J. Wildland Fire* **2005**, *14*, 189–198. [CrossRef]
173. Kokaly, R.F.; Rockwell, B.W.; Haire, S.L.; King, T.V.V. Characterization of post-fire surface cover, soils, and burn severity at the Cerro Grande Fire, New Mexico, using hyperspectral and multispectral remote sensing. *Remote Sens. Environ.* **2007**, *106*, 305–325. [CrossRef]
174. Loboda, T.; O'Neal, K.J.; Csiszar, I. Regionally adaptable dNBR-based algorithm for burned area mapping from MODIS data. *Remote Sens. Environ.* **2007**, *109*, 429–442. [CrossRef]
175. Allen, J.L.; Sorbel, B. Assessing the differenced Normalized Burn Ratio's ability to map burn severity in the boreal forest and tundra ecosystems of Alaska's national parks. *Int. J. Wildland Fire* **2008**, *17*, 463–475. [CrossRef]
176. van Wagtendonk, J.W.; Root, R.R.; Key, C.H. Comparison of AVIRIS and Landsat ETM+ detection capabilities for burn severity. *Remote Sens. Environ.* **2004**, *92*, 397–408. [CrossRef]
177. Burton, P.J.; Parisien, M.A.; Hicke, J.A.; Hall, R.J.; Freeburn, J.T. Large fires as agents of ecological diversity in the North American boreal forest. *Int. J. Wildland Fire* **2008**, *17*, 754–767. [CrossRef]
178. García-Martín, A.; Pérez-Cabello, F.; de la Riva Fernández, J.; Llovería, R.M. Estimation of crown biomass of Pinus spp. from Landsat TM and its effect on burn severity in a Spanish fire scar. *IEEE J. Sel. Top. Appl. Earth Obs. Remote Sens.* **2008**, *1*, 254–265. [CrossRef]
179. Godwin, D.R.; Kobziar, L.N. Comparison of burn severities of consecutive large-scale fires in Florida sand pine scrubusing satellite imagery analysis. *Fire Ecol.* **2011**, *7*, 99–113. [CrossRef]
180. Picotte, J.J.; Robertson, K. Timing constraints on remote sensing of wildland fire burned area in the southeastern US. *Remote Sens.* **2011**, *3*, 1680–1690. [CrossRef]
181. Eidenshink, J.C.; Schwind, B.; Brewer, K.; Zhu, Z.L.; Quayle, B.; Howard, S.M. A project for monitoring trends in burn severity. *Fire Ecol.* **2007**, *3*, 3–21. [CrossRef]
182. Tian, L.; Wang, J.; Zhou, H.; Wang, J. Automatic detection of forest fire disturbance based on dynamic modelling from MODIS time-series observations. *Int. J. Remote Sens.* **2018**, *39*, 3801–3815. [CrossRef]
183. Salguero, J.; Li, J.; Farahmand, A.; Reager, J.T. Wildfire trend analysis over the contiguous United States using remote sensing observations. *Remote Sens.* **2020**, *12*, 2565. [CrossRef]
184. Franco, M.G.; Mundo, I.A.; Veblen, T.T. Field-validated burn-severity napping in north Patagonian forests. *Remote Sens.* **2020**, *12*, 214. [CrossRef]
185. Epting, J.; Verbyla, D.; Sorbel, B. Evaluation of remotely sensed indices for assessing burn severity in interior Alaska using Landsat TM and ETM+. *Remote Sens. Environ.* **2005**, *96*, 328–339. [CrossRef]
186. Miller, J.D.; Thode, A.E. Quantifying burn severity in a heterogeneous landscape with a relative version of the delta Normalized Burn Ratio (dNBR). *Remote Sens. Environ.* **2007**, *109*, 66–80. [CrossRef]
187. Potter, C. Ten years of forest cover change in the Sierra Nevada detected using Landsat satellite image analysis. *Int. J. Remote Sens.* **2014**, *35*, 7136–7153. [CrossRef]
188. Miller, J.D.; Quayle, B. Calibration and validation of immediate post-fire satellite-derived data to three severity metrics. *Fire Ecol.* **2015**, *11*, 12–30. [CrossRef]
189. Cansler, C.A.; McKenzie, D. How robust are burn severity indices when applied in a new region? Evaluation of alternate field-based and remote-sensing methods. *Remote Sens.* **2012**, *4*, 456–483. [CrossRef]

190. Norton, J.; Glenn, N.; Germino, M.; Weber, K.; Seefeldt, S. Relative suitability of indices derived from Landsat ETM+ and SPOT 5 for detecting fire severity in sagebrush steppe. *Int. J. Appl. Earth Obs. Geoinf.* **2009**, *11*, 360–367. [CrossRef]
191. Hoy, E.E.; French, N.H.F.; Turetsky, M.R.; Trigg, S.N.; Kasischke, E.S. Evaluating the potential of Landsat TM/ETM+ imagery for assessing fire severity in Alaskan black spruce forests. *Int. J. Wildland Fire* **2008**, *17*, 500–514. [CrossRef]
192. Miller, J.D.; Knapp, E.E.; Key, C.H.; Skinner, C.N.; Isbell, C.J.; Creasy, R.M.; Sherlock, J.W. Calibration and validation of the relative differenced Normalized Burn Ratio (RdNBR) to three measures of fire severity in the Sierra Nevada and Klamath Mountains, California, USA. *Remote Sens. Environ.* **2009**, *113*, 645–656. [CrossRef]
193. Murphy, K.A.; Reynolds, J.H.; Koltun, J.M. Evaluating the ability of the differenced Normalized Burn Ratio (dNBR) to predict ecologically significant burn severity in Alaskan boreal forests. *Int. J. Wildland Fire* **2008**, *17*, 490–499. [CrossRef]
194. Verbyla, D.L.; Kasischke, E.S.; Hoy, E.E. Seasonal and topographic effects on estimating fire severity from Landsat TM/ETM+ data. *Int. J. Wildland Fire* **2008**, *17*, 527–534. [CrossRef]
195. Cai, L.; Wang, M. Is the RdNBR a better estimator of wildfire burn severity than the dNBR? A discussion and case study in southeast China. *Geocarto Int.* **2022**, *37*, 758–772. [CrossRef]
196. Parks, S.A.; Dillon, G.K.; Miller, C. A new metric for quantifying burn severity: The relativized burn ratio. *Remote Sens.* **2014**, *6*, 1827–1844. [CrossRef]
197. Viedma, O.; Chico, F.; Fernández, J.J.; Madrigal, C.; Safford, H.D.; Moreno, J.M. Disentangling the role of prefire vegetation vs. burning conditions on fire severity in a large forest fire in SE Spain. *Remote Sens. Environ.* **2020**, *247*, 111891. [CrossRef]
198. Harvey, B.J.; Andrus, R.A.; Anderson, S.C. Incorporating biophysical gradients and uncertainty into burn severity maps in a temperate fire-prone forested region. *Ecosphere* **2019**, *10*, e02600. [CrossRef]
199. Gallagher, M.R.; Skowronski, N.S.; Lathrop, R.G.; McWilliams, T.; Green, E.J. An improved approach for selecting and validating burn severity indices in forested landscapes. *Can. J. Remote Sens.* **2020**, *46*, 100–111. [CrossRef]
200. Loboda, T.V.; French, N.H.F.; Hight-Harf, C.; Jenkins, L.; Miller, M.E. Mapping fire extent and burn severity in Alaskan tussock tundra: An analysis of the spectral response of tundra vegetation to wildland fire. *Remote Sens. Environ.* **2013**, *134*, 194–209. [CrossRef]
201. Mallinis, G.; Mitsopoulos, I.; Chrysafi, I. Evaluating and comparing Sentinel 2A and Landsat-8 operational land imager (OLI) spectral indices for estimating fire severity in a Mediterranean pine ecosystem of Greece. *GIScience Remote Sens.* **2018**, *55*, 1–18. [CrossRef]
202. Fernández-García, V.; Santamarta, M.; Fernández-Manso, A.; Quintano, C.; Marcos, E.; Calvo, L. Burn severity metrics in fire-prone pine ecosystems along a climatic gradient using Landsat imagery. *Remote Sens. Environ.* **2018**, *206*, 205–217. [CrossRef]
203. Lambin, E.F.; Goyvaerts, K.; Petit, C. Remotely-sensed indicators of burning efficiency of savannah and forest fires. *Int. J. Remote Sens.* **2003**, *24*, 3105–3118. [CrossRef]
204. Lyons, E.; Jin, Y.; Randerson, J. Changes in surface albedo after fire in boreal forest ecosystems of interior Alaska assessed using MODIS satellite observations. *J. Geophys. Res. Biogeosci.* **2008**, *113*, G02012. [CrossRef]
205. Veraverbeke, S.; Verstraeten, W.W.; Lhermitte, S.; Van De Kerchove, R.; Goossens, R. Assessment of post-fire changes in land surface temperature and surface albedo, and their relation with fire—Burn severity using multitemporal MODIS imagery. *Int. J. Wildland Fire* **2012**, *21*, 243–256. [CrossRef]
206. Vlassova, L.; Pérez-Cabello, F.; Mimbrero, M.R.; Llovería, R.M.; García-Martín, A. Analysis of the relationship between land surface temperature and wildfire severity in a series of Landsat images. *Remote Sens.* **2014**, *6*, 6136–6162. [CrossRef]
207. Chen, D.; Loboda, T.V. Surface forcing of non-stand-replacing fires in Siberian larch forests. *Environ. Res. Lett.* **2018**, *13*, 045008. [CrossRef]
208. Mota, B.; Gobron, N.; Cappucci, F.; Morgan, O. Burned area and surface albedo products: Assessment of change consistency at global scale. *Remote Sens. Environ.* **2019**, *225*, 249–266. [CrossRef]
209. Shvetsov, E.G.; Ponomarev, E.I. Postfire effects in Siberian larch stands on multispectral satellite data. *Contemp. Probl. Ecol.* **2020**, *13*, 104–112. [CrossRef]
210. Harris, S.; Veraverbeke, S.; Hook, S. Evaluating spectral indices for assessing fire severity in chaparral ecosystems (Southern California) using MODIS/ASTER (MASTER) airborne simulator data. *Remote Sens.* **2011**, *3*, 2403–2419. [CrossRef]
211. Maffei, C.; Alfieri, S.M.; Menenti, M. Relating spatiotemporal patterns of forest fires burned area and duration to diurnal land surface temperature anomalies. *Remote Sens.* **2018**, *10*, 1777. [CrossRef]
212. Couturier, S.; Taylor, D.; Siegert, F.; Hoffmann, A.; Bao, M.Q. ERS SAR backscatter: A potential real-time indicator of the proneness of modified rainforests to fire. *Remote Sens. Environ.* **2001**, *76*, 410–417. [CrossRef]
213. Gimeno, M.; San-Miguel-Ayanz, J.; Schmuck, G. Identification of burnt areas in Mediterranean forest environments from ERS-2 SAR time series. *Int. J. Remote Sens.* **2004**, *25*, 4873–4888. [CrossRef]
214. Minchella, A.; Del Frate, F.; Capogna, F.; Anselmi, S.; Manes, F. Use of multitemporal SAR data for monitoring vegetation recovery of Mediterranean burned areas. *Remote Sens. Environ.* **2009**, *113*, 588–597. [CrossRef]
215. Polychronaki, A.; Gitas, I.Z.; Veraverbeke, S.; Debien, A. Evaluation of ALOS PALSAR Imagery for Burned Area Mapping in Greece Using Object-Based Classification. *Remote Sens.* **2013**, *5*, 5680–5701. [CrossRef]
216. Tanase, M.A.; Santoro, M.; Wegmüller, U.; de la Riva, J.; Pérez-Cabello, F. Properties of X-, C-and L-band repeat-pass interferometric SAR coherence in Mediterranean pine forests affected by fires. *Remote Sens. Environ.* **2010**, *114*, 2182–2194. [CrossRef]

217. Mari, N.; Laneve, G.; Cadau, E.; Porcasi, X. Fire damage assessment in Sardinia: The use of ALOS/PALSAR data for post fire effects management. *Eur. J. Remote Sens.* **2012**, *45*, 233–241. [CrossRef]
218. Gimeno, M.; San-Miguel-Ayanz, J. Evaluation of RADARSAT-1 data for identification of burnt areas in Southern Europe. *Remote Sens. Environ.* **2004**, *92*, 370–375. [CrossRef]
219. Malenovský, Z.; Rott, H.; Cihlar, J.; Schaepman, M.E.; García-Santos, G.; Fernandes, R.; Berger, M. Sentinels for science: Potential of Sentinel-1, -2, and -3 missions for scientific observations of ocean, cryosphere, and land. *Remote Sens. Environ.* **2012**, *120*, 91–101. [CrossRef]
220. Belenguer-Plomer, M.A.; Tanase, M.A.; Fernandez-Carrillo, A.; Chuvieco, E. Burned area detection and mapping using Sentinel-1 backscatter coefficient and thermal anomalies. *Remote Sens. Environ.* **2019**, *233*, 111345. [CrossRef]
221. Engelbrecht, J.; Theron, A.; Vhengani, L.; Kemp, J. A simple normalized difference approach to burnt area mapping using multi-polarisation C-Band SAR. *Remote Sens.* **2017**, *9*, 764. [CrossRef]
222. Goetz, S.J.; Sunt, M.; Baccini, A.; Beck, P.S.A. Synergistic use of spaceborne lidar and optical imagery for assessing forest disturbance: An Alaska case study. *J. Geophys. Res. Biogeosci.* **2010**, *115*, G00E07. [CrossRef]
223. Beck, P.S.A.; Goetz, S.J.; Mack, M.C.; Alexander, H.D.; Jin, Y.; Randerson, J.T.; Loranty, M.M. The impacts and implications of an intensifying fire regime on Alaskan boreal forest composition and albedo. *Glob. Change Biol.* **2011**, *17*, 2853–2866. [CrossRef]
224. Martín-Alcón, S.; Coll, L.; De Cáceres, M.; Guitart, L.; Cabré, M.; Just, A.; González-Olabarría, J.R. Combining aerial LiDAR and multispectral imagery to assess postfire regeneration types in a Mediterranean forest. *Can. J. For. Res.* **2015**, *45*, 856–866. [CrossRef]
225. Bolton, D.K.; Coops, N.C.; Wulder, M.A. Characterizing residual structure and forest recovery following high-severity fire in the western boreal of Canada using Landsat time-series and airborne LiDAR data. *Remote Sens. Environ.* **2015**, *163*, 48–60. [CrossRef]
226. Wulder, M.A.; White, J.C.; Alvarez, F.; Han, T.; Rogan, J.; Hawkes, B. Characterizing boreal forest wildfire with multi-temporal Landsat and LIDAR data. *Remote Sens. Environ.* **2009**, *113*, 1540–1555. [CrossRef]
227. Kane, V.R.; North, M.P.; Lutz, J.A.; Churchill, D.J.; Roberts, S.L.; Smith, D.F.; McGaughey, R.J.; Kane, J.T.; Brooks, M.L. Assessing fire effects on forest spatial structure using a fusion of Landsat and airborne LiDAR data in Yosemite National Park. *Remote Sens. Environ.* **2014**, *151*, 89–101. [CrossRef]
228. Fernandez-Manso, A.; Quintano, C.; Roberts, D.A. Burn severity analysis in Mediterranean forests using maximum entropy model trained with EO-1 Hyperion and LiDAR data. *ISPRS J. Photogramm. Remote Sens.* **2019**, *155*, 102–118. [CrossRef]
229. García-Llamas, P.; Suárez-Seoane, S.; Taboada, A.; Marcos, E.; Fernández-Manso, A.; Quintano, C.; Fernández-García, V.; Fernández-Guisuraga, J.M.; Calvo, L. Environmental drivers of fire severity in extreme fire events that affect Mediterranean pine forest ecosystems. *For. Ecol. Manag.* **2019**, *433*, 24–32. [CrossRef]
230. McCarley, T.R.; Kolden, C.A.; Vaillant, N.M.; Hudak, A.T.; Smith, A.M.S.; Wing, B.M.; Kellogg, B.S.; Kreitler, J. Multi-temporal LiDAR and Landsat quantification of fire-induced changes to forest structure. *Remote Sens. Environ.* **2017**, *191*, 419–432. [CrossRef]
231. Meng, R.; Wu, J.; Schwager, K.L.; Zhao, F.; Dennison, P.E.; Cook, B.D.; Brewster, K.; Green, T.M.; Serbin, S.P. Using high spatial resolution satellite imagery to map forest burn severity across spatial scales in a Pine Barrens ecosystem. *Remote Sens. Environ.* **2017**, *191*, 95–109. [CrossRef]
232. Bishop, B.D.; Dietterick, B.C.; White, R.A.; Mastin, T.B. Classification of plot-level fire-caused tree mortality in a redwood forest using digital orthophotography and LiDAR. *Remote Sens.* **2014**, *6*, 1954–1972. [CrossRef]
233. Montealegre, A.L.; Lamelas, M.T.; Tanase, M.A.; De la Riva, J. Forest fire severity assessment using ALS data in a Mediterranean environment. *Remote Sens.* **2014**, *6*, 4240–4265. [CrossRef]
234. Liu, M.; Popescu, S.; Malambo, L. Feasibility of burned area mapping based on ICESAT-2 photon counting data. *Remote Sens.* **2020**, *12*, 24. [CrossRef]
235. Brewer, C.K.; Winne, J.C.; Redmond, R.L.; Opitz, D.W.; Mangrich, M.V. Classifying and mapping wildfire severity: A comparison of methods. *Photogramm. Eng. Remote Sens.* **2005**, *71*, 1311–1320. [CrossRef]
236. Bryukhanov, A.V.; Panov, A.V.; Ponomarev, E.I.; Sidenko, N.V. Wildfire impact on the main tree species of the Near-Yenisei Siberia. *Izv. Atmos. Ocean. Phys.* **2018**, *54*, 1525–1533. [CrossRef]
237. Malak, D.A.; Pausas, J.G. Fire regime and post-fire Normalized Difference Vegetation Index changes in the eastern Iberian peninsula (Mediterranean basin). *Int. J. Wildland Fire* **2006**, *15*, 407–413. [CrossRef]
238. Veraverbeke, S.; Gitas, I.; Katagis, T.; Polychronaki, A.; Somers, B.; Goossens, R. Assessing post-fire vegetation recovery using red-near infrared vegetation indices: Accounting for background and vegetation variability. *ISPRS J. Photogramm. Remote Sens.* **2012**, *68*, 28–39. [CrossRef]
239. Fernandez-Manso, A.; Quintano, C.; Roberts, D.A. Burn severity influence on post-fire vegetation cover resilience from Landsat MESMA fraction images time series in Mediterranean forest ecosystems. *Remote Sens. Environ.* **2016**, *184*, 112–123. [CrossRef]
240. Fernández-Guisuraga, J.M.; Suárez-Seoane, S.; Calvo, L. Modeling *Pinus pinaster* forest structure after a large wildfire using remote sensing data at high spatial resolution. *For. Ecol. Manag.* **2019**, *446*, 257–271. [CrossRef]
241. Kotel'nikov, R.V.; Lupyan, E.A.; Bartalev, S.A.; Ershov, D.V. Space monitoring of forest fires: History of the creation and development of ISDM-Rosleskhoz. *Contemp. Probl. Ecol.* **2020**, *13*, 795–802. [CrossRef]
242. Crist, E.P.; Cicone, R.C. A physically-based transformation of thematic mapper data—The TM tasseled cap. *IEEE Trans. Geosci. Remote Sens.* **1984**, *GE-22*, 256–263. [CrossRef]

243. Collins, J.B.; Woodcock, C.E. An assessment of several linear change detection techniques for mapping forest mortality using multitemporal Landsat TM data. *Remote Sens. Environ.* **1996**, *56*, 66–77. [CrossRef]
244. Healey, S.P.; Cohen, W.B.; Zhiqiang, Y.; Krankina, O.N. Comparison of tasseled cap-based Landsat data structures for use in forest disturbance detection. *Remote Sens. Environ.* **2005**, *97*, 301–310. [CrossRef]
245. Song, C.; Schroeder, T.A.; Cohen, W.B. Predicting temperate conifer forest successional stage distributions with multitemporal Landsat Thematic Mapper imagery. *Remote Sens. Environ.* **2007**, *106*, 228–237. [CrossRef]
246. Masek, J.G.; Huang, C.; Wolfe, R.; Cohen, W.; Hall, F.; Kutler, J.; Nelson, P. North American forest disturbance mapped from a decadal Landsat record. *Remote Sens. Environ.* **2008**, *112*, 2914–2926. [CrossRef]
247. Liu, W.; Song, C.; Schroeder, T.A.; Cohen, W.B. Predicting forest successional stages using multitemporal Landsat imagery with forest inventory and analysis data. *Int. J. Remote Sens.* **2008**, *29*, 3855–3872. [CrossRef]
248. Petrakis, R.E.; Villarreal, M.L.; Wu, Z.; Hetzler, R.; Middleton, B.R.; Norman, L.M. Evaluating and monitoring forest fuel treatments using remote sensing applications in Arizona, U.S.A. *For. Ecol. Manag.* **2018**, *413*, 48–61. [CrossRef]
249. Dunn, C.J.; O'Connor, C.D.; Reilly, M.J.; Calkin, D.E.; Thompson, M.P. Spatial and temporal assessment of responder exposure to snag hazards in post-fire environments. *For. Ecol. Manag.* **2019**, *441*, 202–214. [CrossRef]
250. Storey, E.A. Postfire evaluation of fuelwood loss and restoration priority in a mixed, community-managed conifer forest of central New Mexico, United States. *Appl. Geogr.* **2020**, *117*, 102182. [CrossRef]
251. Hicke, J.A.; Asner, G.P.; Kasischke, E.S.; French, N.H.F.; Randerson, J.T.; Collatz, G.J.; Stocks, B.J.; Compton, J.T.; Tucker, C.J.; Los, S.O.; et al. Postfire response of North American boreal forest net primary productivity analyzed with satellite observations. *Glob. Change Biol.* **2003**, *9*, 1145–1157. [CrossRef]
252. Goetz, S.J.; Fiske, G.J.; Bunn, A.G. Using satellite time-series data sets to analyze fire disturbance and forest recovery across Canada. *Remote Sens. Environ.* **2006**, *101*, 352–365. [CrossRef]
253. Cuevas-Gonzalez, M.; Gerard, F.; Balzter, H.; Riano, D. Studying the change in fAPAR after forest fires in Siberia using MODIS. *Int. J. Remote Sens.* **2008**, *29*, 6873–6892. [CrossRef]
254. Epting, J.; Verbyla, D. Landscape-level interactions of prefire vegetation, burn severity, and postfire vegetation over a 16-year period in interior Alaska. *Can. J. For. Res.* **2005**, *35*, 1367–1377. [CrossRef]
255. Frazier, R.J.; Coops, N.C.; Wulder, M.A.; Hermosilla, T.; White, J.C. Analyzing spatial and temporal variability in short-term rates of post-fire vegetation return from Landsat time series. *Remote Sens. Environ.* **2018**, *205*, 32–45. [CrossRef]
256. Mitchell, M.; Yuan, F. Assessing forest fire and vegetation recovery in the black hills, South Dakota. *GIScience Remote Sens.* **2010**, *47*, 276–299. [CrossRef]
257. Bastos, A.; Gouveia, C.M.; Dacamara, C.C.; Trigo, R.M. Modelling post-fire vegetation recovery in Portugal. *Biogeosciences* **2011**, *8*, 3593–3607. [CrossRef]
258. Hayes, J.J.; Robeson, S.M. Relationships between fire severity and post-fire landscape pattern following a large mixed-severity fire in the Valle Vidal, New Mexico, USA. *For. Ecol. Manag.* **2011**, *261*, 1392–1400. [CrossRef]
259. Polychronaki, A.; Gitas, I.Z.; Minchella, A. Monitoring post-fire vegetation recovery in the Mediterranean using SPOT and ERS imagery. *Int. J. Wildland Fire* **2014**, *23*, 631–642. [CrossRef]
260. Krylov, A.; McCarty, J.C.; Potapov, P.; Loboda, T.; Tyukavina, A.; Turubanova, S.; Hansen, M.C. Remote sensing estimates of stand-replacement fires in Russia, 2002–2011. *Environ. Res. Lett.* **2014**, *9*, 105007. [CrossRef]
261. Di Mauro, B.; Fava, F.; Busetto, L.; Crosta, G.F.; Colombo, R. Post-fire resilience in the Alpine region estimated from MODIS satellite multispectral data. *Int. J. Appl. Earth Obs. Geoinf.* **2014**, *32*, 163–172. [CrossRef]
262. Vlassova, L.; Pérez-Cabello, F. Effects of post-fire wood management strategies on vegetation recovery and land surface temperature (LST) estimated from Landsat images. *Int. J. Appl. Earth Obs. Geoinf.* **2016**, *44*, 171–183. [CrossRef]
263. Chu, T.; Guo, X.; Takeda, K. Remote sensing approach to detect post-fire vegetation regrowth in Siberian boreal larch forest. *Ecol. Indic.* **2016**, *62*, 32–46. [CrossRef]
264. Fava, F.; Colombo, R. Remote sensing-based assessment of the 2005–2011 bamboo reproductive event in the Arakan mountain range and its relation with wildfires. *Remote Sens.* **2017**, *9*, 85. [CrossRef]
265. Chu, T.; Guo, X.; Takeda, K. Effects of burn severity and environmental conditions on post-fire regeneration in Siberian Larch forest. *Forests* **2017**, *8*, 76. [CrossRef]
266. Li, X.; Zhang, H.; Yang, G.; Ding, Y.; Zhao, J. Post-fire vegetation succession and surface energy fluxes derived from remote sensing. *Remote Sens.* **2018**, *10*, 1000. [CrossRef]
267. Bondur, V.G.; Tsidilina, M.N.; Cherepanova, E.V. Satellite monitoring of wildfire impacts on the conditions of various types of vegetation cover in the federal districts of the Russian Federation. *Izv. Atmos. Ocean. Phys.* **2019**, *55*, 1238–1253. [CrossRef]
268. Yi, K.; Tani, H.; Zhang, J.; Guo, M.; Wang, X.; Zhong, G. Long-term satellite detection of post-fire vegetation trends in boreal forests of China. *Remote Sens.* **2013**, *5*, 6938–6957. [CrossRef]
269. Hope, A.; Albers, N.; Bart, R. Characterizing post-fire recovery of fynbos vegetation in the Western Cape Region of South Africa using MODIS data. *Int. J. Remote Sens.* **2012**, *33*, 979–999. [CrossRef]
270. Caccamo, G.; Bradstock, R.; Collins, L.; Penman, T.; Watson, P. Using MODIS data to analyse post-fire vegetation recovery in Australian eucalypt forests. *J. Spat. Sci.* **2015**, *60*, 341–352. [CrossRef]
271. Yang, J.; Pan, S.; Dangal, S.; Zhang, B.; Wang, S.; Tian, H. Continental-scale quantification of post-fire vegetation greenness recovery in temperate and boreal North America. *Remote Sens. Environ.* **2017**, *199*, 277–290. [CrossRef]

272. Santana, N.C.; Júnior, O.A.d.C.; Gomes, R.A.T.; Fontes Guimarães, R. Comparison of post-fire patterns in Brazilian savanna and tropical forest from remote sensing time series. *ISPRS Int. J. Geo-Inf.* **2020**, *9*, 659. [CrossRef]
273. Ryu, J.-H.; Han, K.-S.; Hong, S.; Park, N.-W.; Lee, Y.-W.; Cho, J. Satellite-Based Evaluation of the Post-Fire Recovery Process from the Worst Forest Fire Case in South Korea. *Remote Sens.* **2018**, *10*, 918. [CrossRef]
274. Meng, R.; Dennison, P.E.; Huang, C.; Moritz, M.A.; D'Antonio, C. Effects of fire severity and post-fire climate on short-term vegetation recovery of mixed-conifer and red fir forests in the Sierra Nevada Mountains of California. *Remote Sens. Environ.* **2015**, *171*, 311–325. [CrossRef]
275. Lee, R.J.; Chow, T.E. Post-wildfire assessment of vegetation regeneration in Bastrop, Texas, using Landsat imagery. *GIScience Remote Sens.* **2015**, *52*, 609–626. [CrossRef]
276. Viana-Soto, A.; Aguado, I.; Salas, J.; García, M. Identifying post-fire recovery trajectories and driving factors using Landsat time series in fire-prone Mediterranean pine forests. *Remote Sens.* **2020**, *12*, 1499. [CrossRef]
277. Sever, L.; Leach, J.; Bren, L. Remote sensing of post-fire vegetation recovery; a study using Landsat 5 TM imagery and NDVI in North-East Victoria. *J. Spat. Sci.* **2012**, *57*, 175–191. [CrossRef]
278. Christopoulou, A.; Mallinis, G.; Vassilakis, E.; Farangitakis, G.-P.; Fyllas, N.M.; Kokkoris, G.D.; Arianoutsou, M. Assessing the impact of different landscape features on post-fire forest recovery with multitemporal remote sensing data: The case of Mount Taygetos (southern Greece). *Int. J. Wildland Fire* **2019**, *28*, 521–532. [CrossRef]
279. Bisson, M.; Fornaciai, A.; Coli, A.; Mazzarini, F.; Pareschi, M.T. The Vegetation Resilience After Fire (VRAF) index: Development, implementation and an illustration from central Italy. *Int. J. Appl. Earth Obs. Geoinf.* **2008**, *10*, 312–329. [CrossRef]
280. Zhao, F.R.; Meng, R.; Huang, C.; Zhao, M.; Zhao, F.A.; Gong, P.; Yu, L.; Zhu, Z. Long-term post-disturbance forest recovery in the greater yellowstone ecosystem analyzed using Landsat time series stack. *Remote Sens.* **2016**, *8*, 898. [CrossRef]
281. Malak, D.A.; Pausas, J.G.; Pardo-Pascual, J.E.; Ruiz, L.A. Fire recurrence and the dynamics of the Enhanced Vegetation Index in a Mediterranean ecosystem. *Int. J. Appl. Geospatial. Res.* **2015**, *6*, 18–35. [CrossRef]
282. Kuplich, T.M. Classifying regenerating forest stages in Amazonia using remotely sensed images and a neural network. *For. Ecol. Manag.* **2006**, *234*, 1–9. [CrossRef]
283. Huesca, M.; Merino-de-Miguel, S.; González-Alonso, F.; Martínez, S.; Cuevas, J.M.; Calle, A. Using AHS hyper-spectral images to study forest vegetation recovery after a fire. *Int. J. Remote Sens.* **2013**, *34*, 4025–4048. [CrossRef]
284. Domingo, D.; de la Riva, J.; Lamelas, M.T.; García-Martín, A.; Ibarra, P.; Echeverría, M.; Hoffrén, R. Fuel type classification using airborne laser scanning and Sentinel 2 data in Mediterranean forest affected by wildfires. *Remote Sens.* **2020**, *12*, 3660. [CrossRef]
285. Hoffman, K.M.; Trant, A.J.; Nijland, W.; Starzomski, B.M. Ecological legacies of fire detected using plot-level measurements and LiDAR in an old growth coastal temperate rainforest. *For. Ecol. Manag.* **2018**, *424*, 11–20. [CrossRef]
286. Pádua, L.; Guimarães, N.; Adão, T.; Sousa, A.; Peres, E.; Sousa, J.J. Effectiveness of Sentinel-2 in multi-temporal post-fire monitoring when compared with UAV Imagery. *ISPRS Int. J. Geo-Inf.* **2020**, *9*, 225. [CrossRef]
287. Carreiras, J.M.B.; Jones, J.; Lucas, R.M.; Shimabukuro, Y.E. Mapping major land cover types and retrieving the age of secondary forests in the Brazilian Amazon by combining single-date optical and radar remote sensing data. *Remote Sens. Environ.* **2017**, *194*, 16–32. [CrossRef]
288. Attarchi, S.; Gloaguen, R. Classifying complex mountainous forests with L-Band SAR and Landsat data integration: A comparison among different machine learning methods in the Hyrcanian forest. *Remote Sens.* **2014**, *6*, 3624–3647. [CrossRef]
289. Sato, L.Y.; Gomes, V.C.F.; Shimabukuro, Y.E.; Keller, M.; Arai, E.; Dos-Santos, M.N.; Brown, I.F.; Aragão, L.E.O.e.C.d. Post-fire changes in forest biomass retrieved by airborne LiDAR in Amazonia. *Remote Sens.* **2016**, *8*, 839. [CrossRef]
290. Gordon, C.E.; Price, O.F.; Tasker, E.M. Mapping and exploring variation in post-fire vegetation recovery following mixed severity wildfire using airborne LiDAR. *Ecol. Appl.* **2017**, *27*, 1618–1632. [CrossRef]
291. Vogeler, J.C.; Yang, Z.; Cohen, W.B. Mapping post-fire habitat characteristics through the fusion of remote sensing tools. *Remote Sens. Environ.* **2016**, *173*, 294–303. [CrossRef]
292. Meng, R.; Wu, J.; Zhao, F.; Cook, B.D.; Hanavan, R.P.; Serbin, S.P. Measuring short-term post-fire forest recovery across a burn severity gradient in a mixed pine-oak forest using multi-sensor remote sensing techniques. *Remote Sens. Environ.* **2018**, *210*, 282–296. [CrossRef]
293. Bolton, D.K.; Coops, N.C.; Hermosilla, T.; Wulder, M.A.; White, J.C. Assessing variability in post-fire forest structure along gradients of productivity in the Canadian boreal using multi-source remote sensing. *J. Biogeogr.* **2017**, *44*, 1294–1305. [CrossRef]
294. Lu, D.; Weng, Q. A survey of image classification methods and techniques for improving classification performance. *Int. J. Remote Sens.* **2007**, *28*, 823–870. [CrossRef]
295. García-Haro, F.J.; Gilabert, M.A.; Meliá, J. Monitoring fire-affected areas using Thematic Mapper data. *Int. J. Remote Sens.* **2001**, *22*, 533–549. [CrossRef]
296. Henry, M.C.; Yool, S.R. Assessing relationships between forest spatial patterns and fire history with fusion of optical and microwave remote sensing. *Geocarto Int.* **2004**, *19*, 25–37. [CrossRef]
297. Henry, M.C. Comparison of single-and multi-date Landsat data for mapping wildfire scars in Ocala National Forest, Florida. *Photogramm. Engin. Remote Sens.* **2008**, *74*, 881–891. [CrossRef]
298. Phua, M.-H.; Tsuyuki, S.; Soo Lee, J.; Ghani, M.A.A. Simultaneous detection of burned areas of multiple fires in the tropics using multisensor remote-sensing data. *Int. J. Remote Sens.* **2012**, *33*, 4312–4333. [CrossRef]

299. Dragozi, E.; Gitas, I.Z.; Stavrakoudis, D.G.; Theocharis, J.B. Burned area mapping using support vector machines and the FuzCoC feature selection method on VHR IKONOS imagery. *Remote Sens.* **2014**, *6*, 12005–12036. [CrossRef]
300. Siljander, M. Predictive fire occurrence modelling to improve burned area estimation at a regional scale: A case study in East Caprivi, Namibia. *Int. J. Appl. Earth Obs. Geoinf.* **2009**, *11*, 380–393. [CrossRef]
301. Potter, C.; Li, S.; Huang, S.; Crabtree, R.L. Analysis of sapling density regeneration in Yellowstone National Park with hyperspectral remote sensing data. *Remote Sens. Environ.* **2012**, *121*, 61–68. [CrossRef]
302. Arnett, J.T.T.R.; Coops, N.C.; Daniels, L.D.; Falls, R.W. Detecting forest damage after a low-severity fire using remote sensing at multiple scales. *Int. J. Appl. Earth Obs. Geoinf.* **2015**, *35*, 239–246. [CrossRef]
303. Brown, D.R.N.; Jorgenson, M.T.; Kielland, K.; Verbyla, D.L.; Prakash, A.; Koch, J.C. Landscape effects of wildfire on permafrost distribution in interior Alaska derived from remote sensing. *Remote Sens.* **2016**, *8*, 654. [CrossRef]
304. Rozario, P.F.; Madurapperuma, B.D.; Wang, Y. Remote sensing approach to detect burn severity risk zones in Palo Verde National Park, Costa Rica. *Remote Sens.* **2018**, *10*, 1427. [CrossRef]
305. Román-Cuesta, R.M.; Retana, J.; Gracia, M.; Rodríguez, R. A quantitative comparison of methods for classifying burned areas with LISS-III imagery. *Int. J. Remote Sens.* **2005**, *26*, 1979–2003. [CrossRef]
306. Lima, A.; Silva, T.S.F.; de Aragão, L.E.O.C.; de Feitas, R.M.; Adami, M.; Formaggio, A.R.; Shimabukuro, Y.E. Land use and land cover changes determine the spatial relationship between fire and deforestation in the Brazilian Amazon. *Appl. Geogr.* **2012**, *34*, 239–246. [CrossRef]
307. Sofan, P.; Vetrita, Y.; Yulianto, F.; Khomarudin, M.R. Multi-temporal remote sensing data and spectral indices analysis for detection tropical rainforest degradation: Case study in Kapuas Hulu and Sintang districts, West Kalimantan, Indonesia. *Nat. Hazards* **2016**, *80*, 1279–1301. [CrossRef]
308. Quintano, C.; Shimabukuro, Y.E.; Fernández, A.; Delgado, J.A. A spectral unmixing approach for mapping burned areas in Mediterranean countries. *Int. J. Remote Sens.* **2005**, *26*, 1493–1498. [CrossRef]
309. Quintano, C.; Fernández-Manso, A.; Fernández-Manso, O.; Shimabukuro, Y.E. Mapping burned areas in Mediterranean countries using spectral mixture analysis from a uni-temporal perspective. *Int. J. Remote Sens.* **2006**, *27*, 645–662. [CrossRef]
310. Roldán-Zamarrón, A.; Merino-de-Miguel, S.; González-Alonso, F.; García-Gigorro, S.; Cuevas, J.M. Minas de Riotinto (south Spain) forest fire: Burned area assessment and fire severity mapping using Landsat 5-TM, Envisat-MERIS, and Terra-MODIS postfire images. *J. Geophys. Res. Biogeosci.* **2006**, *111*, G04S11. [CrossRef]
311. Montorio, R.; Pérez-Cabello, F.; Borini Alves, D.; García-Martín, A. Unitemporal approach to fire severity mapping using multispectral synthetic databases and Random Forests. *Remote Sens. Environ.* **2020**, *249*, 112025. [CrossRef]
312. Quintano, C.; Fernández-manso, A.; Roberts, D.A. Enhanced burn severity estimation using fine resolution ET and MESMA fraction images with machine learning algorithm. *Remote Sens. Environ.* **2020**, *244*, 111815. [CrossRef]
313. Solans Vila, J.P.; Barbosa, P. Post-fire vegetation regrowth detection in the Deiva Marina region (Liguria-Italy) using Landsat TM and ETM+ data. *Ecol. Model.* **2010**, *221*, 75–84. [CrossRef]
314. Sunar, F.; Özkan, C. Forest fire analysis with remote sensing data. *Int. J. Remote Sens.* **2001**, *22*, 2265–2277. [CrossRef]
315. Malone, S.L.; Kobziar, L.N.; Staudhammer, C.L.; Abd-Elrahman, A. Modeling relationships among 217 fires using remote sensing of burn severity in southern pine forests. *Remote Sens.* **2011**, *3*, 2005–2028. [CrossRef]
316. Pleniou, M.; Koutsias, N. Sensitivity of spectral reflectance values to different burn and vegetation ratios: A multi-scale approach applied in a fire affected area. *ISPRS J. Photogramm. Remote Sens.* **2013**, *79*, 199–210. [CrossRef]
317. Shin, J.-I.; Seo, W.-W.; Kim, T.; Park, J.; Woo, C.-S. Using UAV multispectral images for classification of forest burn severity-A case study of the 2019 Gangneung forest fire. *Forests* **2019**, *10*, 1025. [CrossRef]
318. Picos, J.; Alonso, L.; Bastos, G.; Armesto, J. Event-based integrated assessment of environmental variables and wildfire severity through Sentinel-2 Data. *Forests* **2019**, *10*, 1021. [CrossRef]
319. De Oliveira, L.N.; Lazzarini, G.M.J.; Batista, A.C.; De Lima Fonseca Alves, K.C.C.; Giongo, M. Use of multispectral imaging in the evaluation of burnings and forest fires in Krahôlandia indigenous land (2003–2014). *Floresta* **2015**, *45*, 853–864. [CrossRef]
320. Roy, D.P.; Kumar, S.S. Multi-year MODIS active fire type classification over the Brazilian tropical moist forest biome. *Int. J. Digit. Earth.* **2017**, *10*, 54–84. [CrossRef]
321. Ramo, R.; García, M.; Rodríguez, D.; Chuvieco, E. A data mining approach for global burned area mapping. *Int. J. Appl. Earth Obs. Geoinf.* **2018**, *73*, 39–51. [CrossRef]
322. Janssen, T.A.J.; Ametsitsi, G.K.; Collins, M.; Adu-Bredu, S.; Oliveras, I.; Mitchard, E.T.; Veenendaal, E.M. Extending the baseline of tropical dry forest loss in Ghana (1984–2015) reveals drivers of major deforestation inside a protected area. *Biol. Conserv.* **2018**, *218*, 163–172. [CrossRef]
323. Klauberg, C.; Hudak, A.T.; Silva, C.A.; Lewis, S.A.; Robichaud, P.R.; Jain, T.B. Characterizing fire effects on conifers at tree level from airborne laser scanning and high-resolution, multispectral satellite data. *Ecol. Model.* **2019**, *412*, 108820. [CrossRef]
324. Keyser, A.R.; Westerling, A.L.R. Predicting increasing high severity area burned for three forested regions in the western United States using extreme value theory. *For. Ecol. Manag.* **2019**, *432*, 694–706. [CrossRef]
325. Shang, C.; Wulder, M.A.; Coops, N.C.; White, J.C.; Hermosilla, T. Spatially-explicit prediction of wildfire burn probability using remotely-sensed and ancillary data. *Can. J. Remote Sens.* **2020**, *46*, 313–329. [CrossRef]
326. Gibson, R.; Danaher, T.; Hehir, W.; Collins, L. A remote sensing approach to mapping fire severity in south-eastern Australia using Sentinel 2 and random forest. *Remote Sens. Environ.* **2020**, *240*, 111702. [CrossRef]

327. Collins, L.; McCarthy, G.; Mellor, A.; Newell, G.; Smith, L. Training data requirements for fire severity mapping using Landsat imagery and random forest. *Remote Sens. Environ.* **2020**, *245*, 111839. [CrossRef]
328. Gómez, I.; Martin, M.P. Prototyping an artificial neural network for burned area mapping on a regional scale in Mediterranean areas using MODIS images. *Int. J. Appl. Earth Obs. Geoinf.* **2011**, *13*, 741–752. [CrossRef]
329. Sedano, F.; Kempeneers, P.; Strobl, P.; McInerney, D.; San Miguel, J. Increasing spatial detail of burned scar maps using IRS-AWiFS data for Mediterranean Europe. *Remote Sens.* **2012**, *4*, 726–744. [CrossRef]
330. Pereira-Pires, J.E.; Aubard, V.; Ribeiro, R.A.; Fonseca, J.M.; Silva, J.M.N.; Mora, A. Semi-automatic methodology for fire break maintenance operations detection with sentinel-2 imagery and artificial neural network. *Remote Sens.* **2020**, *12*, 909. [CrossRef]
331. Gutiérrez-Velez, V.H.; Uriarte, M.; DeFries, R.; Pinedo-Vásquez, M.; Fernandes, K.; Ceccato, P.; Baethgen, W.; Padoch, C. Land cover change interacts with drought severity to change fire regimes in Western Amazonia. *Ecol. Appl.* **2014**, *24*, 1323–1340. [CrossRef]
332. Zhan, X.; Sohlberg, R.A.; Townshend, J.R.G.; DiMiceli, C.; Carroll, M.L.; Eastman, J.C.; Hansen, M.C.; DeFries, R.S. Detection of land cover changes using MODIS 250 m data. *Remote Sens. Environ.* **2002**, *83*, 336–350. [CrossRef]
333. Maeda, E.E.; Arcoverde, G.F.B.; Pellikka, P.K.E.; Shimabukuro, Y.E. Fire risk assessment in the Brazilian Amazon using MODIS imagery and change vector analysis. *Appl. Geogr.* **2011**, *31*, 76–84. [CrossRef]
334. Guindon, L.; Bernier, P.Y.; Beaudoin, A.; Pouliot, D.; Villemaire, P.; Hall, R.J.; Latifovic, R.; St-Amant, R. Annual mapping of large forest disturbances across Canada's forests using 250 m MODIS imagery from 2000 to 2011. *Can. J. For. Res.* **2014**, *44*, 1545–1554. [CrossRef]
335. Cardille, J.A.; Fortin, J.A. Bayesian updating of land-cover estimates in a data-rich environment. *Remote Sens. Environ.* **2016**, *186*, 234–249. [CrossRef]
336. Crowley, M.A.; Cardille, J.A.; White, J.C.; Wulder, M.A. Generating intra-year metrics of wildfire progression using multiple open-access satellite data streams. *Remote Sens. Environ.* **2019**, *232*, 111295. [CrossRef]
337. Fernández-Guisuraga, J.M.; Calvo, L.; Fernández-García, V.; Marcos-Porras, E.; Taboada, Á.; Suárez-Seoane, S. Efficiency of remote sensing tools for post-fire management along a climatic gradient. *For. Ecol. Manag.* **2019**, *433*, 553–562. [CrossRef]
338. Petropoulos, G.P.; Kontoes, C.; Keramitsoglou, I. Burnt area delineation from a uni-temporal perspective based on Landsat TM imagery classification using Support Vector Machines. *Int. J. Appl. Earth Obs. Geoinf.* **2011**, *13*, 70–80. [CrossRef]
339. Corbane, C.; Carrion, D.; Broglia, M. Development and implementation of a validation protocol for crisis maps: Reliability and consistency assessment of burnt area maps. *Int. J. Digit. Earth.* **2011**, *4*, 8–24. [CrossRef]
340. Viedma, O. The influence of topography and fire in controlling landscape composition and structure in Sierra de Gredos (Central Spain). *Landsc. Ecol.* **2008**, *23*, 657–672. [CrossRef]
341. Leon, J.R.R.; van Leeuwen, W.J.D.; Casady, G.M. Using MODIS-NDVI for the modeling of post-wildfire vegetation response as a function of environmental conditions and pre-fire restoration treatments. *Remote Sens.* **2012**, *4*, 598–621. [CrossRef]
342. Morgan, P.; Hudak, A.T.; Wells, A.; Parks, S.A.; Baggett, L.S.; Bright, B.C.; Green, P. Multidecadal trends in area burned with high severity in the Selway-Bitterroot Wilderness Area 1880–2012. *Int. J. Wildland Fire* **2017**, *26*, 930–943. [CrossRef]
343. Hawbaker, T.J.; Vanderhoof, M.K.; Beal, Y.-J.; Takacs, J.D.; Schmidt, G.L.; Falgout, J.T.; Williams, B.; Fairaux, N.M.; Caldwell, M.K.; Picotte, J.J.; et al. Mapping burned areas using dense time-series of Landsat data. *Remote Sens. Environ.* **2017**, *198*, 504–522. [CrossRef]
344. Viedma, O.; Torres, I.; Pérez, B.; Moreno, J.M. Modeling plant species richness using reflectance and texture data derived from QuickBird in a recently burned area of Central Spain. *Remote Sens. Environ.* **2012**, *119*, 208–221. [CrossRef]
345. Alencar, A.; Asner, G.P.; Knapp, D.; Zarin, D. Temporal variability of forest fires in eastern Amazonia. *Ecol. Appl.* **2011**, *21*, 2397–2412. [CrossRef]
346. Huang, S.; Liu, H.; Dahal, D.; Jin, S.; Welp, L.R.; Liu, J.; Liu, S. Modeling spatially explicit fire impact on gross primary production in interior Alaska using satellite images coupled with eddy covariance. *Remote Sens. Environ.* **2013**, *135*, 178–188. [CrossRef]
347. Unnikrishnan, A.; Reddy, C.S. Characterizing distribution of forest fires in Myanmar using Earth observations and spatial statistics tool. *J. Indian Soc. Remote Sens.* **2020**, *48*, 227–234. [CrossRef]
348. Pulvirenti, L.; Squicciarino, G.; Fiori, E.; Fiorucci, P.; Ferraris, L.; Negro, D.; Gollini, A.; Severino, M.; Puca, S. An automatic processing chain for near real-time mapping of burned forest areas using Sentinel-2 data. *Remote Sens.* **2020**, *12*, 674. [CrossRef]
349. Satish, K.V.; Reddy, C.S. Long term monitoring of forest fires in Silent Valley National Park, Western Ghats, India using remote sensing data. *J. Indian Soc. Remote Sens.* **2016**, *44*, 207–215. [CrossRef]
350. Bowman, D.M.J.S.; Walsh, A.; Prior, L.D. Landscape analysis of Aboriginal fire management in Central Arnhem Land, north Australia. *J. Biogeogr.* **2004**, *31*, 207–223. [CrossRef]
351. Harcombe, P.A.; Greene, S.E.; Kramer, M.G.; Acker, S.A.; Spies, T.A.; Valentine, T. The influence of fire and windthrow dynamics on a coastal spruce-hemlock forest in Oregon, USA, based on aerial photographs spanning 40 years. *For. Ecol. Manag.* **2004**, *194*, 71–82. [CrossRef]
352. Chuvieco, E.; Ventura, G.; Martín, M.P.; Gómez, I. Assessment of multitemporal compositing techniques of MODIS and AVHRR images for burned land mapping. *Remote Sens. Environ.* **2005**, *94*, 450–462. [CrossRef]
353. Silva, J.M.N.; Sá, A.C.L.; Pereira, J.M.C. Comparison of burned area estimates derived from SPOT-VEGETATION and Landsat ETM+ data in Africa: Influence of spatial pattern and vegetation type. *Remote Sens. Environ.* **2005**, *96*, 188–201. [CrossRef]

354. Holden, Z.A.; Smith, A.M.S.; Morgan, P.; Rollins, M.G.; Gessler, P.E. Evaluation of novel thermally enhanced spectral indices for mapping fire perimeters and comparisons with fire atlas data. *Int. J. Remote Sens.* **2005**, *26*, 4801–4808. [CrossRef]
355. Gong, P.; Pu, R.; Li, Z.; Scarborough, J.; Clinton, N.; Levien, L.M. An integrated approach to wildland fire mapping of California, USA using NOAA/AVHRR data. *Photogramm. Eng. Remote Sens.* **2006**, *72*, 139–150. [CrossRef]
356. Vega-García, C.; Chuvieco, E. Applying local measures of spatial heterogeneity to Landsat-TM images for predicting wildfire occurrence in Mediterranean landscapes. *Landsc. Ecol.* **2006**, *21*, 595–605. [CrossRef]
357. Hammill, K.A.; Bradstock, R.A. Remote sensing of fire severity in the Blue Mountains: Influence of vegetation type and inferring fire intensity. *Int. J. Wildland Fire* **2006**, *15*, 213–226. [CrossRef]
358. González-Alonso, F.; Merino-De-Miguel, S.; Roldán-Zamarrón, A.; García-Gigorro, S.; Cuevas, J.M. MERIS full resolution data for mapping level-of-damage caused by forest fires: The Valencia de Alcántara event in August 2003. *Int. J. Remote Sens.* **2007**, *28*, 797–809. [CrossRef]
359. Loboda, T.V.; Csiszar, I.A. Reconstruction of fire spread within wildland fire events in Northern Eurasia from the MODIS active fire product. *Glob. Planet. Change* **2007**, *56*, 258–273. [CrossRef]
360. Pocewicz, A.; Vierling, L.A.; Lentile, L.B.; Smith, R. View angle effects on relationships between MISR vegetation indices and leaf area index in a recently burned ponderosa pine forest. *Remote Sens. Environ.* **2007**, *107*, 322–333. [CrossRef]
361. Kodandapani, N.; Cochrane, M.A.; Sukumar, R. A comparative analysis of spatial, temporal, and ecological characteristics of forest fires in seasonally dry tropical ecosystems in the Western Ghats, India. *For. Ecol. Manag.* **2008**, *256*, 607–617. [CrossRef]
362. Fox, D.M.; Maselli, F.; Carrega, P. Using SPOT images and field sampling to map burn severity and vegetation factors affecting post forest fire erosion risk. *Catena* **2008**, *75*, 326–335. [CrossRef]
363. Koutsias, N.; Pleniou, M.; Mallinis, G.; Nioti, F.; Sifakis, N.I. A rule-based semi-automatic method to map burned areas: Exploring the USGS historical Landsat archives to reconstruct recent fire history. *Int. J. Remote Sens.* **2013**, *34*, 7049–7068. [CrossRef]
364. Tian, X.; Zhao, F.; Shu, L.; Wang, M. Distribution characteristics and the influence factors of forest fires in China. *For. Ecol. Manag.* **2013**, *310*, 460–467. [CrossRef]
365. Fernández-Manso, A.; Quintano, C. A synergetic approach to burned area mapping using maximum entropy modeling trained with hyperspectral data and VIIRS hotspots. *Remote Sens.* **2020**, *12*, 858. [CrossRef]
366. Liu, S.; Zheng, Y.; Dalponte, M.; Tong, X. A novel fire index-based burned area change detection approach using Landsat-8 OLI data. *Eur. J. Remote Sens.* **2020**, *53*, 104–112. [CrossRef]
367. Liu, Z.; Yang, J.; Dwomoh, F. Mapping recent burned patches in Siberian larch forest using Landsat and MODIS data. *Eur. J. Remote Sens.* **2016**, *49*, 861–887. [CrossRef]
368. Mithal, V.; Nayak, G.; Khandelwal, A.; Kumar, V.; Nemani, R.; Oza, N.C. Mapping burned areas in tropical forests using a novel machine learning framework. *Remote Sens.* **2018**, *10*, 69. [CrossRef]
369. Blaschke, T. Object-based image analysis for remote sensing. *ISPRS J. Photogramm. Remote Sens.* **2010**, *65*, 2–16. [CrossRef]
370. Phua, M.-H.; Tsuyuki, S.; Lee, J.S.; Sasakawa, H. Detection of burned peat swamp forest in a heterogeneous tropical landscape: A case study of the Klias Peninsula, Sabah, Malaysia. *Landsc. Urban Plan.* **2007**, *82*, 103–116. [CrossRef]
371. Gitas, I.Z.; Mitri, G.H.; Ventura, G. Object-based image classification for burned area mapping of Creus Cape, Spain, using NOAA-AVHRR imagery. *Remote Sens. Environ.* **2004**, *92*, 409–413. [CrossRef]
372. Mitri, G.H.; Gitas, I.Z. A performance evaluation of a burned area object-based classification model when applied to topographically and non-topographically corrected TM imagery. *Int. J. Remote Sens.* **2004**, *25*, 2863–2870. [CrossRef]
373. Mitri, G.H.; Gitas, I.Z. Fire type mapping using object-based classification of Ikonos imagery. *Int. J. Wildland Fire* **2006**, *15*, 457–462. [CrossRef]
374. Gitas, I.Z.; Polychronaki, A.; Katagis, T.; Mallinis, G. Contribution of remote sensing to disaster management activities: A case study of the large fires in the Peloponnese, Greece. *Int. J. Remote Sens.* **2008**, *29*, 1847–1853. [CrossRef]